Materials Science & Engineering C 118 (2021) 111360

Contents lists available at ScienceDirect

Materials Science & Engineering C

journal homepage: www.elsevier.com/locate/msec

Efficient non-contact heat generation on flexible, ternary hydroxyapatite/curdlan/nanomagnetite hybrids for temperature controlled processes

Magdalena Kulpa-Greszta[a,*], Robert Pązik[b,*], Patrycja Kłoda[a], Anna Tomaszewska[b], Emilia Zachanowicz[c], Krzysztof Pałka[d], Grazyna Ginalska[e,f], Anna Belcarz[e,f]

[a] Faculty of Chemistry, Rzeszow University of Technology, Aleja Powstańców Warszawy 12, 35-959 Rzeszow, Poland
[b] Department of Biotechnology, Institute of Biology and Biotechnology, College of Natural Sciences, University of Rzeszow, Pigonia 1, 35-310 Rzeszow, Poland
[c] Polymer Engineering and Technology Division, Wroclaw University of Technology, 50-370 Wrocław, Poland
[d] Faculty of Mechanical Engineering, Lublin University of Technology, Nadbystrzycka 36, 20-618 Lublin, Poland
[e] Chair and Department of Biochemistry and Biotechnology, Medical University of Lublin, Chodzki 1, 20-093 Lublin, Poland
[f] Medical Inventi Joint stock Company, 14 Nałęczowska Str., 20-701 Lublin, Poland

ARTICLE INFO

Keywords:
Multifunctional biocomposites
Bone regeneration processes
Heat induction
Ferrites
Magnetite

ABSTRACT

The ternary HAp/curdlan/nanomagnetite hybrids with ceramic and polymer phase incorporation of magnetite nanoparticles (MNPs) were fabricated to study their heating ability under action of the alternating magnetic field (AMF), 808 nm near infrared laser radiation (NIR) and their synergic stimulation. The energy conversion was evaluated in terms of the specific absorption rate (*SAR*) as a function of the MNPs concentration in composites and to estimate their potential in temperature-controlled regenerative processes and hyperthermia. Measurements were carried out on dry and Ringer's solution soaked composite materials in order to mimic *in situ* conditions. It was found that the MNPs release during prolonged experiment is limited and has no significant effect on energy conversion emphasizing stability of the hybrids. Incorporation of the MNPs in polymer phase of the hybrid can additionally limit particle leaking as well as plays a role as insulating layer for the heat dissipation lowering the risk of sample overheating. In general, it was shown that maximum temperature of hybrid can be achieved in a relatively short time of exposure to stimulating factors whereas its control can be done through optimization of experiment conditions. MNPs incorporation into the curdlan (polymer phase) lead to strengthening of the mechanical properties of the whole network.

1. Introduction

Ceramic composites based on the hydroxyapatite ($Ca_{10}(PO_4)_6(OH)_2$ – HAp), tricalcium phosphate ($Ca_3(PO_4)_2$ – α and β-TCP) and biphasic calcium phosphates (BCP) containing different ratio of HAp/β-TCP are commonly used as the bone substitute/replacement materials [1,2] in orthopedic and maxillofacial surgery [3–5]. The BCP bioceramics are of growing interests allowing for control of biodegradation speed and bioactivity. This can be realized due to the fact that the more soluble β-TCP undergoes much faster resorption leading to easier deposition of apatites in contrast to HAp [6]. However, overall enhancement of properties of the ceramic biomaterials can be achieved by combining powders or granules with synthetic and/or preferably natural polymers. Another possibility relies on addition of other substances which can result in increased biological functionality and improved therapeutic potential. This can be done through enrichment of the polymeric/HAp composite with magnetite nanoparticles (Fe_3O_4 – hereafter MNPs) showing strong ferromagnetic or superparamagnetic behavior depending on their particle size, distribution and aggregation state [7,8]. These types of compounds upon action of alternating magnetic field (AMF) and irradiated with the NIR laser light exhibit several physical properties among which heat generation is the most important one [9]. This material responsivity can be successfully utilized in the heat-stimulated/triggered regenerative processes of bone tissue [10–12]. Moreover, direct sample irradiation with NIR light from the spectral range covering so called biological optical windows can reduce interaction with illuminated tissues due to the minimized absorption and for the same reason allow for deeper light penetration [13]. The MNPs incorporated directly into the bone-replacement materials/hybrids/scaffolds can act on several important levels – can stimulate and alter mechanism of bone formation and treatment of diseases especially upon utilization of their magnetic properties and outcomes coming from the

* Corresponding authors.
E-mail addresses: d436@stud.prz.edu.pl (M. Kulpa-Greszta), rpazik@ur.edu.pl (R. Pązik).

https://doi.org/10.1016/j.msec.2020.111360
Received 1 May 2020; Received in revised form 13 July 2020; Accepted 3 August 2020
Available online 11 August 2020
0928-4931/ © 2020 Elsevier B.V. All rights reserved.

AMF stimulation resulting in possibility of inducing temperature effects. On the other hand one can also take advantage of MNPs optical properties related to the absorption of NIR light to further enhance the temperature effect and combine both approaches to propose magneto-optical-hyperthermia/temperature treatment [10]. It was already reported that the heat induction can stimulate bone regeneration processes through significant stimulation of osteogenesis, enhanced alkaline phosphatase expression in osteoblastic cells or improved cellular adhesion [12].

In the case of the AMF, temperature of the magnetic material can increase due to the contribution of three mechanisms (1) losses related to the coercive field and magnetic hysteresis, (2) losses caused by generation of the eddy currents and (3) residual losses understood as the inner Neel relaxation (reorientation of magnetic spins within particle) and outer Brownian relaxation (movement of the whole particle forced by the changing magnetic field) [14]. These effects can be quite strong and lead to the increase of temperature of biological system above 43 °C (hyperthermia or even ablation) inducing controlled cell apoptosis for instance [15]. In turn, if temperature system is below 41 °C (diathermia regime) stimulation of regenerative and therapeutic processes are possible as well (vasodilation and enhancement of transport properties) [13]. Recently, it was shown that the HAp bioactive scaffolds enriched with Resovist® (commercial Fe_3O_4 coated with carboxydextran) effectively stimulated formation of the new bone without side effects through promotion of the osteogenesis [12]. Such behavior opens promising treatment of bone tissue-related diseases/defects. Interaction of the monochromatic NIR radiation with ferrite magnetic material results in light absorption and consecutive spontaneous non-radiative relaxation causing material heating [16,17]. Both stimulations are non-contact and can be used for localized and specific heat induction of tissues. The simultaneous action of both factors, with different physical mechanisms involved, may give a superior effect on the heat generation [9].

Recently, studies devoted to the ternary bioactive composites/hybrids composed of calcium phosphate ceramics and natural polymers amended with nanoparticles showing magnetic functionality are of particular importance for regenerative medicine [18–25]. Another interesting application is sought in wastewater treatment systems for removal of heavy metals or toxic dyes contamination due to the strong adsorption ability of MNPs and large surface area of highly porous microstructure of composite [26,27]. In multicomponent hybrids for bone defects, ceramic HAp intensifies osteoconductivity, whereas polymeric substance plays a role of an agent which remarkably enhances mechanical properties and biocompatibility. Incorporation of the MNPs into composite is seen as an another added value resulting in formation of multifunctional platform giving possibility of active and multidimensional support in regeneration of bone tissue or even effective elimination of neoplastic cells through hyperthermia [19,20,22,25]. In recent studies both effect of the static magnetic field (STM) [22,28] and AMF are of increased interest in this class of composite materials [10–12,19,24,28–31]. Currently, in the ternary bone scaffolds most commonly used natural macromolecular compounds are collagen [19,22,32], cellulose [20] and chitosan [23,26,33]. The hybrids based on the β-1,3-glucan (curdlan) and HAp with MNPs modification have not been studied yet. However, binary composite of the HAp/curdlan was already proposed by us in the treatment of the bone fracture/defects in animal and human patients [34–36]. We have proven that this type of scaffold is characterized by the high plasticity, elasticity, surgical handiness, good soaking capacity, capability of drug uptake and release as well as high bioactivity [37–39]. In this composite, hydroxyapatite ceramics (92 w/w%) plays a role of strength-providing bioactive and osteoconductive compound. Curdlan (8 w/w%) is a biocompatible matrix which combines the ceramic granules into one compact mass and ensures its elasticity and flexibility when the composite is soaked in water, buffered solution, drug solutions or blood, serum and plasma. Therefore, the modification of such promising biomaterial with magnetic nanoparticles can result in a new functional properties and broaden its possible applications. The main goal of current studies was focused on evaluation of the heat generation effectiveness of the MNPs embedded into the HAp/curdlan hybrid under stimulation of AMF, the 808 nm NIR laser radiation (minimized radiation absorption and scattering in a biological media) and synergistic action of both for the potential use in a temperature-controlled bone tissue regenerative processes. Mechanical properties of composites were studied in order to reveal the effect of the MNPs incorporation either in HAp and curdlan phase. The prolonged studies of the MNPs release were performed in different media to check whether there is a possible particle transfer into the biological media as well.

2. Experimental

2.1. Synthesis of magnetic nanoparticles

The ferrite nanoparticles (Fe_3O_4) were synthesized using the protocol described by us previously [40,41]. The Fe_3O_4 were prepared by thermal decomposition of 6 mmol $Fe(acac)_3$ (iron (III) acetylacetonate; 99.7%, Thermo Fischer Scientific, Germany) in 70 ml acetophenone as a solvent (99%, Sigma Aldrich, Poland). In order to prevent iron complex from unwanted deterioration all manipulations with chemicals were performed in the acrylic glove box (GS Glove Box Systemtechnik GMBH P10R250T2 – automatic gas pressure control) under inert nitrogen atmosphere (99.999%, Linde, Poland). The reaction was carried out in a one neck glass flask equipped with a reflux condenser/column at the boiling temperature of acetophenone (202 °C) for 4 h. Afterwards, the dark brown product was separated and purified through repeated centrifugation and ethyl alcohol washing cycles (eight times) until characteristic scent of acetophenone completely vanished. The final concentration of the MNPs alcohol stock dispersion (13.6 mg/ml) was determined using a microbalance technique. Reasonable part of the colloid was dried until dry mass and used for the characterization of physicochemical properties (XRD, FT-IR-ATR, TGA) whereas rest of the MNPs were used either for the DLS, TEM and served as a main source in fabrication of the ternary HAp/curdlan/magnetite hybrids. Heat induction effectiveness was measured by using 1 mg/ml MNPs water dispersion (deionized H_2O fulfilling Pharmacopoeia requirements) using different types of stimulation (AMF and NIR radiation).

2.2. Fabrication of ternary HAp/curdlan/nanomagnetite composites

The hydroxyapatite (HAp) granules for the preparation of composites (porosity: 67%), were synthesized according to the procedure described in the patent [42] for Medical Inventi Joint stock Company (Lublin, Poland). Briefly, ceramic powder was synthesized by wet chemical precipitation technique (Ca/P molar ratio: 1.67). 1.67 mol H_3PO_4 (85%, Avantor, Poland) was added to dispersed 1 mol $Ca(OH)_2$ (95%, Chempur, Poland) suspended in deionized water, under constant stirring, at 25 °C and pH of the suspension was adjusted to 11 by NaOH solution (98%, Avantor, Poland). The precipitate was subjected to aging for 4 days, then washed with distilled water, dried, calcined at 800 °C for 2 h and sieved to obtain the granules of 0.2–0.3 mm and 0.4–0.6 mm fraction. The natural polymer β-1,3-glucan (curdlan) from *Alcaligenes faecalis* (DP 450) was supplied by Wako Chemicals (Japan). The MNPs were directly taken as a nanoparticle ethanol stock solution (13.6 mg/ml) as described in the previous section.

2.2.1. Preparation of the reference binary composite

The binary composite were synthesized as previously described [37,38] with a permission obtained from the Medical Inventi Joint stock Company (owner of the intellectual property for the HAp/curdlan composite). Briefly, reference samples were prepared by combining 3.4 g of the HAp porous granules (mixture of two fractions: 0.2–0.3 mm and 0.4–0.6 mm in the weight ratio of 25:75) with the 5 ml of aqueous

suspension containing 0.4 g of the curdlan. The resulting mixture was thermally treated at 93 °C for 15 min in the special cylinder-shaped molds and cut into cylinders with the diameters of ø 8 mm and 8 mm length (for mechanical tests), ø 13 mm and 10 mm length (other tests). Afterwards scaffolds were dried at 25 °C for 48 h. Further binary hybrids were sterilized in the plastic/paper peel pouch by using ethylene oxide sterilization at 55 °C for 1 h and finally were left for 20 h of aeration.

Ternary HAp/curdlan/MNPs hybrids were fabricated by two distinctly different approaches: (I) by the MNPs incorporation into ceramics phase and (II) MNPs incorporation into polymer (curdlan) phase.

(I) Preparation of the ternary composite with MNPs incorporated into HAp phase

Prior to the composite preparation, MNPs were introduced into HAp granular phase. For this purpose, appropriate amounts of nanoparticle ethanol stock solution (13.6 mg/ml) were mixed with water to obtain the solutions of final volume of 3.66 ml. The concentrations of MNPs suspensions were calculated in a way that the final weight/weight ratio of the MNPs (mg) *vs*. HAp and curdlan (g) in composite samples were 0.75 mg/g (1), 1 mg/g (2), 1.25 mg/g (3), 1.5 mg/g (4), 1.75 mg/g (5) and 2 mg/g (6), respectively. These solutions were evenly spread into portions (3.4 g) of HAp granules (mixture of two fractions: 0.2–0.3 mm and 0.4–0.6 mm in the weight ratio of 25:75) and left for the evaporation at 37 °C until stable dry mass was obtained. Dried granules were combined with 5 ml of aqueous suspensions containing 0.4 g of the curdlan and treated according to the procedure described for the reference sample, including sterilization, without any further changes.

(II) Preparation of the ternary composite with MNPs incorporated into polymer (curdlan) phase

Incorporation of the MNPs into polymer phase was done by mixing of the aqueous suspension containing 0.4 g of the curdlan with appropriate amounts of nanoparticle ethanol stock solution (13.6 mg/ml) to the final volume of 5 ml. The suspension was then combined with 3.4 g of HAp granules and treated according to the procedure described for the reference sample, including sterilization, without any further changes. Depending on a sample, the amounts of MNPs stock solution added to curdlan suspensions were calculated in a way that the final weight/weight ratio of the MNPs (mg) *vs*. HAp and curdlan (g) in composite samples were 0.75 mg/g (1), 1 mg/g (2), 1.25 mg/g (3), 1.5 mg/g (4), 1.75 mg/g (5) and 2 mg/g (6), respectively.

2.3. Characterization of physicochemical properties of MNPs, HAp and ternary hybrids

The X-ray powder diffraction technique (XRD) was used in order to verify the formation and crystal structure of the desired MNPs, HAp granules, curdlan and composites. The measurements were carried out on a Bruker D8 Advanced diffractometer with X-ray source copper lamp ($K_{\alpha 1}$: 1.54060 Å) within 2Θ range of 15–70°. In addition, a Ni filter was utilized in order to filter-out $K_{\alpha 2}$ reflections. Resulting diffraction patterns were compared with the reference cards from the JCPDS database.

MNPs and HAp primary size and morphology, as well as selective area electron diffraction (SAED) were evaluated and determined by transmission electron microscopy (TEM) on a Tecnai Osiris X-FEG HRTEM microscope operating at 200 kV. Sample for the TEM characterization was prepared by taking a droplet of 0.25 mg/ml ethanol based colloidal suspension of Fe_3O_4 and HAp. Materials were deposited on a carbon coated copper grid and dried at room temperature.

Hydrodynamic size of nanoparticles was characterized by dynamic light scattering method (DLS) using Nanoplus HD 3 set-up (Particulate System/Micrometrics) equipped with 660 nm laser diode and autotitrator system. The working concentration of the MNPs giving reliable results was between 30 and 60 μg/ml (water dilution made out of 1 mg/ml stock dispersion). MNPs colloidal stability was determined by measuring the zeta potential (ζ) exploiting the electrophoretic light scattering technique (ELS). For this purpose all dilutions of MNPs were prepared with 0.001 M KCl electrolyte in order to provide even distribution of the electric field. The data was analyzed using dedicated software developed by the instrument manufacturer.

Microstructure of the cross-sectioned ternary hybrids and the reference composite was evaluated by inverted optical microscope Nikon Eclipse MA200. The 50× magnification was applied and images were collected with the same exposure time (38 ms).

Fourier transform infrared spectroscopy technique (FT-IR) was employed for materials characterization with a Thermo Scientific Nicolet iZ10 spectrometer. The spectra were recorded in the range of 4000–500 cm^{-1} at room temperature using attenuated total reflection accessory (ATR). All samples *i.e*. MNPs, HAp, binary and ternary composites were grinded in an agate mortar and placed on a surface of the ATR accessory.

Thermogravimetric (TGA) analysis was carried out on a TA Instruments Q50 V20.13 (precision ± 0.01% and sensitivity 0.1 μg). Small amounts of reference calcium oxalate monohydrate ($Ca(COO)_2{\cdot}H_2O$) and MNPs sample were placed in platinum vessels. The equipment prior experiment was calibrated by two-points temperature calibration. Instrument validity was tested with decomposition process of reference. After that, sample containing MNPs was heated under inert gas flow (N_2 6 dm^3/h), at a rate of 5 °C/min from 25 up to 900 °C. Obtained data was analyzed with Universal V4.5 software to determine mass change, residue mass and temperature of the decomposition process.

Diffuse reflectance spectra of samples were performed on Carry 5000 UV-VIS-NIR spectrophotometer (Agilent Technologies) equipped with internal DRA 2500 accessory. Prior measurement all samples were grinded into powders and directly measured using mentioned accessory.

Specific heat capacity measurements were performed by Differential Scanning Calorimetry system (DSC) (Mettler Toledo), coupled with Huber TC 100 intracooler. Before the DSC survey, all composites were conditioned in a vacuum dryer at 60 °C for 24 h. After that, samples (~7.5 mg) were measured in the 40 ml aluminum pans under a constant nitrogen purge (60 ml/min) from 10 °C to 90 °C with the heating rate 1 °C/min using TOPEM® modulated procedure. Each measurement was repeated three times to achieve satisfactory statistics and exclude errors connected with measuring artifacts. Experimental data was processed using the generic STARe software.

Heat generation ability of MNPs colloid, ternary hybrids as well as reference binary composite induced by the alternating magnetic field (AMF) and near-infrared laser radiation (NIR) was carried out on a G2 D5 Series Multimode 1500 W driver (nanoScale Biomagnetics, Spain) equipped with CAL1 (calorimetric measurement) and S32 coilsets. The specific absorption rate (*SAR*) was evaluated on MNPs colloid and composite samples to estimate the material properties in terms of effectiveness of energy conversion.

Composites characterization was carried out on S32 coilset (see Fig. 1) and PC70 (see supplementary file Fig. S7) mimicking *in vivo* application. The G2 driver (alternating magnetic field generator) is able to generate a magnetic field with following parameters: field frequency 100–771 kHz and field intensity within the range of 3.8–34.5 kA/m. Both settings depend on each other. In the case of NIR stimulation 808 nm continuous wave laser module equipped with 400 μm optical fiber (CNI, China) was used. The laser source offers control over broad range of laser power up to the maximum of 2.4 W with power stability no worse than 1%. Direct effect of the AMF action and NIR radiation was recorded by FLIR T660 thermovision camera and analyzed with ResearchIR dedicated software. Ternary hybrids and reference composite were placed inside an S32 coilset using special sample holder assuring 100% magnetic field coverage. The entire measuring module

Fig. 1. Set-up for measurement of the heat induction on hybrids using AMF and NIR laser (G2 generator with insulated S32 coil).

was thermally isolated by a thick-walled polystyrene box filled with additional polymer based foam insulating material. Heat generation capability was tested by application of both stimuli AMF and NIR separately and simultaneously (dual mode). The sample cooling stage after suspended action of AMF and NIR was also recorded for chosen composites. In each particular case, optimization of AMF and NIR settings was conducted. Heat conversion experiments were repeated three times for different content of MNPs (0.75 up to 2 mg/g of composites with MNPs incorporated into HAp or polymer). Additionally, PC70 planar coilset extended with the external chamber with input and output sockets for water thermalization was used for simulation of the internal body temperature ~37 °C on chosen samples (data in the supplementary file). Detailed specification of the coilsets in terms of magnetic field distribution, field frequency and intensity can be found in the supplementary file. In the case of most responsive hybrids, tests in close-to-biological environment conditions were performed using Ringer's solution. Composites were immersed in a Ringer fluid for 30 min at room temperature to allow the complete soaking and placed in measuring set-up. Data analysis and *SAR* calculation was done with OriginPro 2018b software (OriginLab, USA).

Mechanical behavior of the tested binary and ternary hybrids during compression was evaluated on samples measuring 8 mm in diameter and 8 mm in length. Before the measurements samples were immersed in Ringer's solution containing 10% of human serum and 1% of Antibiotic Antimycotic solution (Sigma-Aldrich, USA) for 24 h to ensure the full soaking. The Autograph AG-X plus universal testing machine (Shimadzu, Japan) was used to conduct compression testing with two different crosshead rates of 0.5 mm/min and 10 mm/min on two individual sets of samples. It was expected that the difference in deformation rate would show the viscoelastic nature of the materials tested. All measurements started after obtaining a force value of 0.1 N to eliminate clearance between the sample and the holders. The mechanical compression was carried out until 30% of strain was reached. Then the traverse was stopped and the force was still measured within 3 min time to evaluate relaxation behavior. A force sensor with an accuracy of 0.01 N was used. The data obtained in compressive test allowed to calculate the compressive strength σ_c, equal the maximum stress reached at 30% strain, and Young's modulus as well. The relaxation test enabled to determine the non-relaxed relative stress (σ_w), calculated as the ratio of non-relaxed stress measured after 3 min of relaxation (σ_t) to maximum stress observed (σ_c). For each measurement 5 specimens were used. Results were statistically evaluated using unpaired *t*-test at the significance level $\alpha < 0.05$.

2.4. MNPs release from the ternary HAp/curdlan/MNPs hybrids

Sterilized samples of ternary hybrids, in triplicate, obtained both according to method (I) and (II) (see Section 2.2.), were incubated in sterile Sorenson's phosphate buffer with pH 6.5 or 7.4, additionally enriched with 1% Antibiotic-Antimycotic solution (Sigma-Aldrich, USA) to prevent the growth of bacteria and fungi (in proportion 10 ml of buffer per 1 g of dry hybrid weight). Samples were incubated using hematology roller (5 rpm; RM 5, Ingenieurbüro CAT, M. Zipperer GmbH, Germany) at 37 °C for duration of 6 weeks. Portions of buffer solution were aseptically collected every 7th day from each sample and their absorbance was measured at 370 nm, with pure buffer as a reference, using Genesys 10S UV-VIS spectrophotometer equipped with VisionLiteTM v.4.0 software (ThermoScientific, USA). The concentration of the MNPs released from the ternary composites to buffers was calculated on the basis of calibration curve of known Fe_3O_4 MNPs concentrations suspended in the ultrapure water. Finally, the total quantity of MNPs released by hybrids was calculated as a percentage of initial MNPs amount in hybrids. Image of dry ternary hybrid composites after 6 weeks of incubation in buffers was collected using Olympus E-520 camera (Olympus, Japan) for macro photography.

To evaluate the effect of serum proteins on MNPs release profile from ternary hybrids, the samples of composites (containing 1 mg MNPs/g of dry hybrid) weight were incubated in Ringer solution supplemented with 10% human serum (serum was kindly donated by Regional Blood Donation and Blood Treatment Center in Lublin, Poland) and 1% Antibiotic-Antimycotic solution (Sigma-Aldrich, USA) in proportion 10 ml of buffer per 1 g of dry hybrid weight. Then samples were incubated using hematology roller (5 rpm; RM 5, Ingenieurbüro CAT, M. Zipperer GmbH, Germany) at 37 °C for 10 days. Portions of the solution were aseptically collected every second day from each sample and their absorbance was measured at 370 nm, with fresh serum-supplemented Ringer solution as a reference. The concentration of the MNPs released from the ternary composites to serum-supplemented Ringer solution was calculated as described above.

3. Results and discussion

3.1. Physicochemical characterization of materials

3.1.1. Structural and morphological features of MNPs

Structural purity of the Fe_3O_4 nanoparticles prepared under non-hydrolytic approach was confirmed by the XRD powder diffraction technique (see Fig. 2a) through direct comparison with the reference card no. 19-0629 taken from the JCPDS database. It is obvious that the experimental result matches very well with the peak positions of the Bragg's reflections emphasizing that the obtained pattern perfectly corresponds with the cubic structure belonging to the space group. No other peaks related to the presence of impurities were detected. The average crystallite size *D* was calculated using well known Scherrer's equation:

$$D = \frac{k\lambda}{\cos\Theta\sqrt{\beta^2 - \beta_0^2}}, \quad (1)$$

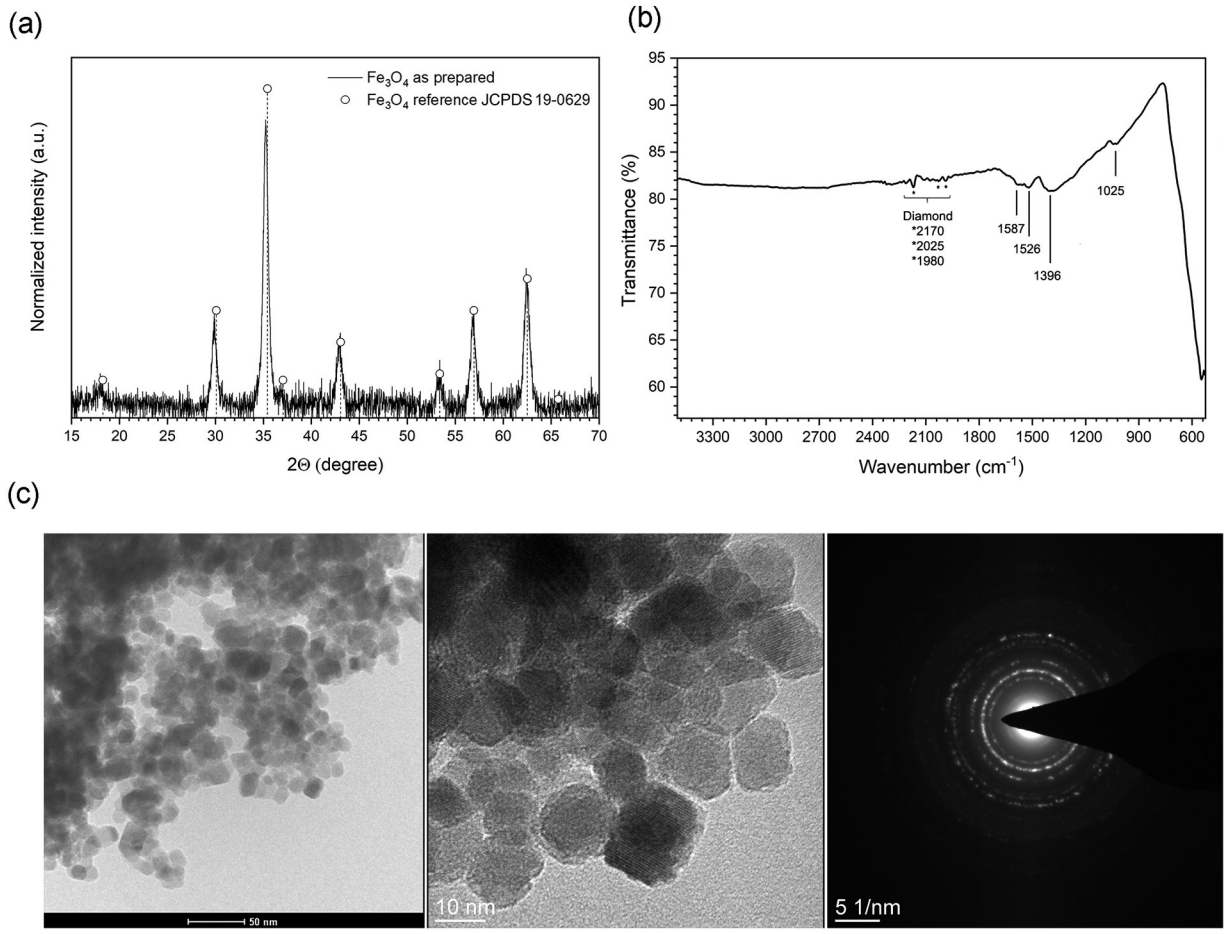

Fig. 2. X-ray powder diffraction pattern (a); FT-IR-ATR spectra (b); as well as TEM and SAED images (c) of the Fe_3O_4 nanoparticles prepared under non-hydrolytic conditions.

where *k* is a constant (here 0.9 – approximation of the spherical particle shape), λ is an X-ray wavelength (1.54060 Å), β_o is ascribed to the apparatus broadening; β is a full width at half maximum of the respective reflection (FWHM) and represents the angle at which maximum peak position chosen for the analysis was located (peak at around 29.9 2Θ was taken) [43]. In the case of the prepared MNPs calculated crystallite size was 12 nm. It gives a very rough image regarding real crystallite size and does not contain any information on the size distribution being an important feature sometimes with critical influence.

The FT-IR-ATR spectrum was measured for the synthesized MNPs (Fig. 2b) in order to check how the applied synthetic protocol shapes surface of the particles. It was also treated as an additional confirmation of the Fe_3O_4 phase formation. As it is clearly seen the recorded spectra reveals presence of several bands with the distinct peak of high intensity located at 591 cm^{-1}. This band was directly ascribed to the vibrations of the Fe—O units at tetrahedral crystallographic sites which is generally treated as the most characteristic and indicative IR mode for the spinel family [44]. In addition, it was found that the location of extra peaks at 1587, 1526, 1396 and 1025 cm^{-1}, respectively correlates well with structural features characterizing acetylacetonate ligand [45]. Presence of residual organics is a typical consequence of the mechanism of nanoparticle formation in the organic rich media that was explained in detail by Kessler et al. [46].

In terms of MNPs application in the temperature-controlled processes one of the key issues to address are the primary size of particles, hydrodynamic diameter and zeta potential. The particle size and distribution were assessed by the analysis of the TEM images being 12.3 ± 1.6 nm (see Fig. 2c). The morphology of the MNPs is rather regular and contain predominantly slightly elongated nanoparticles. One of the advantages of non-hydrolytic protocols is a better control over dispersity of MNPs in contrast to hydrolytic processes. The SAED picture (see panel in Fig. 2c) shows well developed ring-dot pattern. Measured distances between crystallographic planes are well corresponding with the Fe_3O_4 reference standard confirming sample crystallization in a spinel structure. We also noted that, there is an almost perfect match between Scherrer's size calculation and TEM analysis pointing out on that the nanopowder consists of individual crystallites only. Except estimation of the primary size of particles it is crucial to give also the answer on the hydrodynamic diameter and zeta potential of the particles since all of them have a critical impact on effectiveness of the MNPs heat energy generation [47–49]. Preferably hydrodynamic size should be minimized as possible to reduce magnetic interparticle interactions whereas zeta potential should be high enough to assure sufficient colloidal stability (above 30 mV of absolute value). Usually, in order to prepare stable colloidal suspension of nanoparticles, additives have to be used. This should be done with a great caution to avoid cytotoxic effects. Choice of the proper ligand has to be done very carefully. In the case of our MNPs the hydrodynamic diameter was 110.1 nm with polydispersity index (PdI) of 0.153 and zeta potential (ζ) of the colloid was measured to be −23.4 mV (see supplementary file Figs. S1 and S2). We have to emphasize that no organic molecules were used for MNPs suspension stabilization. Main reason for a good colloidal stability of bare MNPs could be related to the presence of residual organics (as indicated by the FT-IR-ATR spectrum). This is also consistent with our previous observations for other spinel and non-spinel nanoparticles synthesized using similar non-hydrolytic protocol [41,50]. Therefore, TGA analysis was performed in order to estimate the quantity of the remaining ligand being below 5% (see

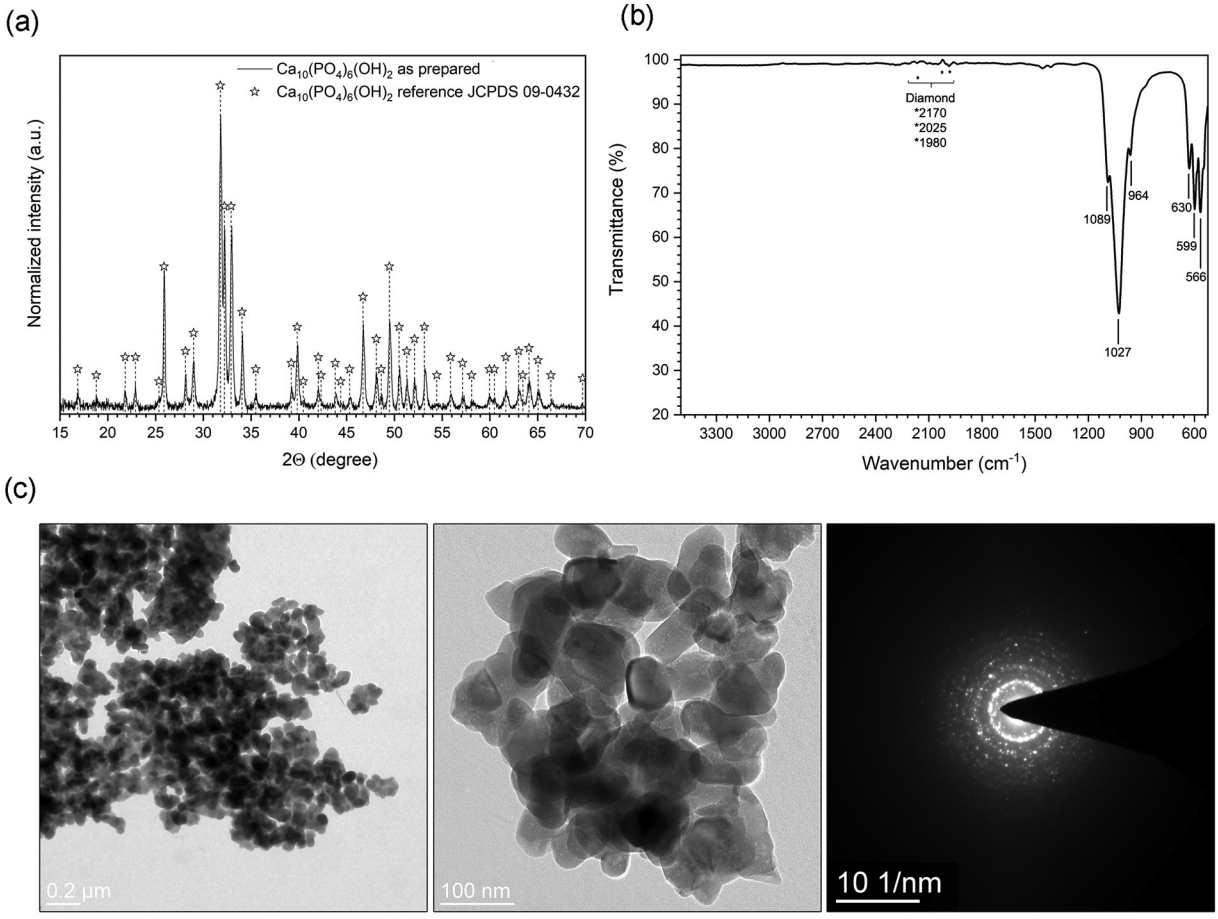

Fig. 3. X-ray powder diffraction pattern (a); FT-IR-ATR spectra (b); as well as TEM and SAED images (c) of the HAp nanoparticles.

supplementary file Fig. S3). In terms of the biological impact we strongly encouraged the reader to familiarize with the results of our previous studies were detailed analysis of MNPs biocompatibility was provided showing no adverse effects [51].

3.1.2. Structural and morphological features of HAp

General characterization of the physiochemical properties of the HAp nanopowders was presented in Fig. 3. Analysis of the structural properties of HAp (Fig. 3a) leads to the conclusion that HAp crystallizes in a hexagonal structure depicted by the $P6_3$ space group as evidenced by the reference standard (JCPDS 09-0432). We did not observe any additional peaks, thus it was assumed that the sample is single phase and highly crystalline since all reflections have significant intensity. The calculated crystallite diameter was around 50 nm and is comparable to that obtained from the TEM characterization. The particle morphology is strongly irregular resembling shapes of other apatites obtained by wet-chemical approaches [52–55]. The FT-IR-ATR spectra shows typical image of the HAp IR active mode vibrations of the PO_4^{3-} units with maxima at 1089, 1027 and 964 cm^{-1} attributed to the ν_3 and ν_4 modes located at 599 and 566 cm^{-1}, respectively. The band at around 630 cm^{-1} results from vibrations of the OH^- groups in hydroxyapatite structure.

3.1.3. Characterization of binary and ternary hybrids

The detailed analysis of the physicochemical properties of binary composites can be found in our previous reports [34–39]. However, for the purpose of this study we compared the structure of all composites by means of the XRD and FT-IR-ATR techniques (Fig. 4) to provide convincing data that during all steps of material fabrication no any changes were induced. It is worth noting, that the XRD pattern of the curdlan shows only a broad peak at low angles characteristic of amorphous material. Incorporation of very small amount of the MNPs (around 0.1%) results in appearance of low intensity peaks at 2Θ corresponding with the two most intense reflections ascribed to the MNPs phase (indicated by two asterisks in Fig. 4). In general, binary and ternary hybrids show only diffraction of the HAp phase. In fact, reflections from this material are that strong so the contribution of polymer to the overall intensity is totally negligible (low S/N ratio, weak intensity, patterns smoothed). In the case of MNPs in ternary hybrids due to low concentration and strong X-ray absorption reflections of ferrite are not visible at all. We have to underline that the detection limit for the XRD is estimated to maximum 3% of phase content. Since, even for the most MNPs concentrated sample it is impossible to measure their presence even though color of the ternary hybrid give a clear evidence of successful MNPs incorporation (see Fig. 5). The same stands for MNPs detection by FT-IR-ATR technique – MNPs concentration is too low and very intense vibrations of HAp cover their signal completely, whereas curdlan alone has an intense band at 600 cm^{-1} being exactly at the position of most characteristic vibrations of the Fe—O bonds. The FT-IR-ATR spectra of curdlan contains characteristic vibration modes being in a perfect agreement with data provided by Rafigh et al. [56] and Kalyanasundaram et al. [57].

The general image of ternary hybrids was presented in Fig. 5. The optical microscopy of ternary hybrids cross sections was used to show the samples microstructure (Fig. 6).

One can clearly distinguish that the white, light-blue areas correspond with the HAp ceramic phase which is covered and surrounded by curdlan as well. The possible reason for such light-blue color of HAp granules is presence of the Mn^{5+} impurities at tetrahedral crystallographic sites of the apatite structure [58] (the order of ppm) showing

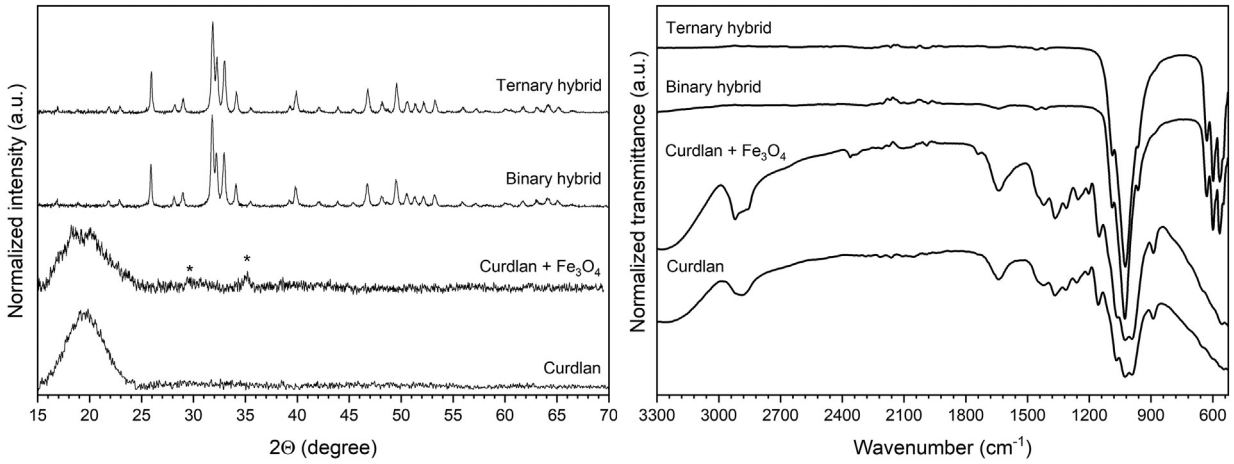

Fig. 4. X-ray powder diffraction pattern (a) and FT-IR-ATR spectra (b) of hybrids.

broad absorption band in the close-to-NIR spectral range (see supplementary file Fig. S4a). The amount of the manganese cations depends strongly on the source of the starting materials, whereas valance state is dictated by the sintering conditions, mainly temperature [59]. The presence of the Mn cations in the HAp might be beneficial due to their effect on activity of osteoblast cells and osteogenesis process. Moreover, it was shown that the HAp doped with Mn cations affects the adherence of the bone cells to the implant material [59,60]. The microstructure of ternary hybrids remain quite the same with significant color difference of hybrids with either HAp- or polymer-incorporated MNPs (Fig. 5). Samples of both types became brownish although hybrids with curdlan-incorporated MNPs were slightly darker. Therefore, it was anticipated that both the presence of the manganese cations in HAp and MNPs incorporation will affect heating performance of ternary hybrids. We also postulated that the polymer coating might work as an insulating layer decreasing heat dissipation.

3.1.4. Effectiveness of heat generation of MNPs colloid under different physical stimulation

The ability to heat generation of MNPs colloidal suspension (1 mg/ml of Fe_3O_4 – standard test concentration) was evaluated by using different stimuli (see Fig. 7). At first, separate exposure to AMF (486 kHz, 22.65 kA/m), 808 nm laser irradiation (481 mW) and synergistic effect of both AMF and NIR to heat conversion (486 kHz, 22.65 kA/m, 481 mW) was studied. In order to calculate the specific absorption rate (*SAR*), treated as a measure of the heating efficiency of the given system, the following expression was taken:

$$SAR = \frac{Cm_{sample}}{m_{NPs}}\frac{dT}{dt}, \quad (2)$$

where C describes the specific heat capacity of sample (J/g°C), m_{sample} is the mass of colloid or hybrid (g), m_{NPs} is the mass of MNPs in a dispersion or in a hybrid (g), dT/dt is the slope of the heating curve fitted with a linear model for the first 30 s of measurement. In the case of the MNPs suspension the water specific heat capacity (4.185 J/g°C) was taken for calculation of *SAR*. Assumption is reasonable since the contribution of the MNPs specific heat capacity to the colloid mass at this MNPs concentration is negligible (0.1%).

In our case, MNPs under action of AMF only shown *SAR* value of 632 W/g (dT/dt – 0.15), for the laser alone 413 W/g (dT/dt – 0.10) and under dual mode it was 760 W/g (dT/dt – 0.18), respectively.

The heating efficacy caused by the AMF on our MNPs is comparable with the latest reports on the magnetic nanoparticles [9]. Thus, we assumed that this colloid with high efficiency of heat generation (high *SAR* value) might be seen as a promising component for the bone replacement material. Upon synergic action of AMF and NIR we did not observe a strong enhancement of colloidal heating ability as compared to the work of Espinoza et al. [9] In addition, Ortgies et al. [61] proposed optomagnetic nanoplatforms (nanocapsules) for *in situ* controlled hyperthermia as well. However, in their report the calculated *SAR* under action of AMF was only 200 W/g (in our case 632 W/g) due to the difference in particle properties (particle size, shape, hydrodynamic size, stability, agglomeration, surface functionalization, ligand type *etc*.) as well as measurement settings (100 kHz, 24 kA/m) in comparison to our MNPs.

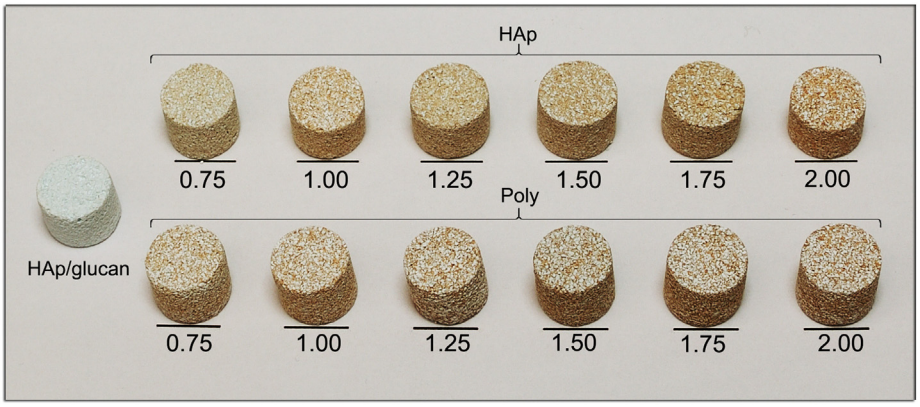

Fig. 5. Control composite (HAp/glucan) and HAp/curdlan/Fe_3O_4 hybrids with different incorporation site (HAp – MNPs incorporated into HAp phase; Poly – MNPs incorporated into curdlan phase) and ratio of MNPs.

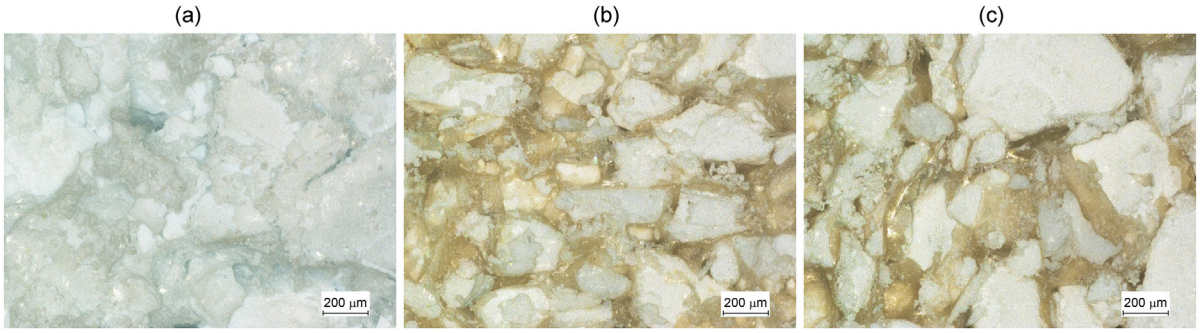

Fig. 6. Optical microscopy images of the cross-sections for reference binary composite (a), hybrid with HAp-incorporated MNPs (b) and hybrid with curdlan-incorporated MNPs (c).

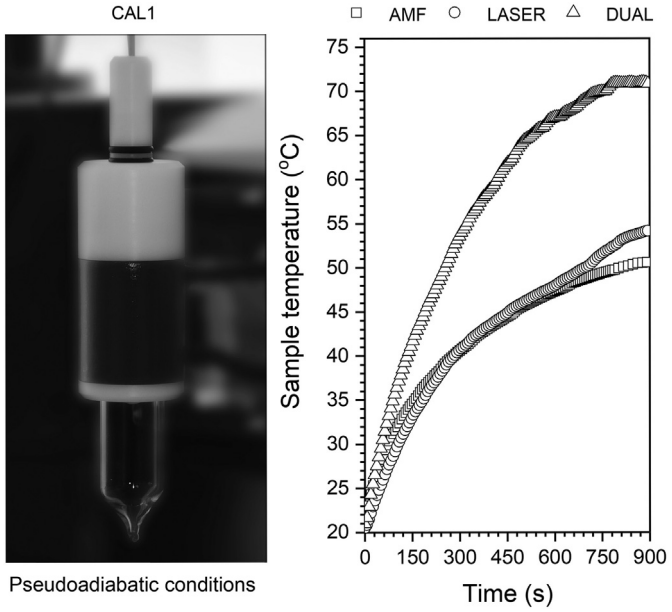

Fig. 7. CAL 1 coilset (left) and heat induction of the Fe_3O_4 TD nanoparticles colloid (1 mg/ml) under different stimulation - AMF, 808 nm laser exposure (LASER) and synergy of both factors (DUAL) (right).

3.1.5. Heat generation on ternary hybrids with different MNPs incorporation into the scaffold microstructure

Heating performance of ternary hybrids induced by the AMF, NIR laser and simultaneous action of both stimuli was assessed thoroughly by the optimization of field frequency, intensity and laser sample distance (optical density). Moreover, effect of the MNPs incorporation phase *i.e.* MNPs in HAp (ceramic phase) or in curdlan (polymer phase) as well as MNPs concentration (0.75–2 mg/g) dependence was examined. Our attention was also focused towards comparison of the heat conversion performed on a dry and wet hybrids. Since the last experimental strategy is not commonly implemented in the literature, we decided to mimic *in situ* conditions through soaking of the samples in protein-free Ringer's solution. As a control, binary composite was used to confirm the outcomes of MNPs utilization in hybrid materials. All measurements were carried out in triplicates showing satisfactory reproducibility. The *SAR* of the hybrids was calculated only for scaffolds with MNPs concentration of 1 mg/g and compared with MNPs colloid, formula (2). The specific heat capacities for ternary hybrids were directly taken from the DSC measurements. They are indicated further in the text as $C_{(I)}$ for MNPs incorporated in HAp (1.08 J/g°C) and $C_{(II)}$ in the polymer phase (1.12 J/g°C). While averaged specific heat capacity (C_{av}) of Ringer's solution soaked composites was calculated using expression shown below:

$$C_{av} = \frac{C_{water} m_{water} + C_{hybrid} m_{hybrid}}{m_{water} + m_{hybrid}}, \quad (3)$$

where C_{hybrid} depending on the MNPs incorporation is equal to $C_{(I)}$ or $C_{(II)}$, m_{water} is the mass of Ringer's solution in composite after soaking and m_{hybrid} is the mass of the given composite [62].

Temperature effects as a function of maximum field intensity for given frequency (factory available presets) were recorded for both type of the MNPs phase incorporation (see supplementary file Fig. S5). Based on the obtained results the optimized magnetic field frequency of 496 kHz (note slight difference between frequencies of both coilsets CAL1 and S32 due to the generator and coils capabilities) and 22 kA/m of field intensity were found for the AMF stimulation. The maximum temperature achieved for dry hybrids containing MNPs loaded into HAp granules was 51 °C, into polymer: 45 °C, whereas Ringer's soaked composites achieved 31 °C and 30 °C depending on the type of incorporation, respectively. Afterwards, we decided to fix the field intensity (22 kA/m) and measure field frequency dependence (Fig. 8a).

One can note that there is a significant change in heating performance upon decrease of the field frequency. Further, optimization of the magnetic field intensity was carried out keeping field frequency at 496 kHz (Fig. 8b). It has been shown that the temperature of the composites can be controlled using broad range of AMF parameters reducing the risk of sample overheating. Another stimulation used for the heat induction was 808 nm laser radiation. For the experiment we selected the laser output power of 481 mW which depending on the distance from the sample is close or slightly above 0.33 W/cm^2 [13]. It was found that increase of the laser distance (Fig. S6) allows for control of the hybrid temperature through decrease of the laser optical density and increase of laser area coverage. What was particularly interesting, we were able to heat up dry ceramics or polymer ternary composites up to 110 °C and 100 °C, respectively. One can note, that the effect of the MNPs phase incorporation is significant. The *SAR* value drops from 632 W/g (MNPs colloidal suspension) up to 421 W/g (MNPs in ceramic phase) and 347 W/g (MNPs in polymeric phase).

Almost two-fold decrease of the MNPs heating efficiency under AMF is caused by nanoparticles immobilization in both phases. It leads to the Brown relaxation (external relaxation) constrain since nanoparticle rotations following magnetic field direction changes are no longer possible [63]. The main implication is that the most probable mechanism of heat generation under AMF is due to the Neel relaxation (internal relaxation – spin reorientations) [64]. We exclude a contribution of the magnetic hysteresis losses because of the particle size (below 13 nm) and their superparamagnetic behavior (no coercivity field) [65]. Variation of *SAR* for MNPs incorporated in ceramic and curdlan phase could be caused by the fact that the polymer forms an insulating layer around MNPs. Therefore, heat dissipation is hindered. Immersion of the composites leads to further decrease of *SAR* due to the medium change with distinctly higher specific heat capacity. Thus, overall temperature increase of hybrids under AMF drops (dT/dt is around 0.06). The *SAR* reaches 382 W/g or 313 W/g depending on

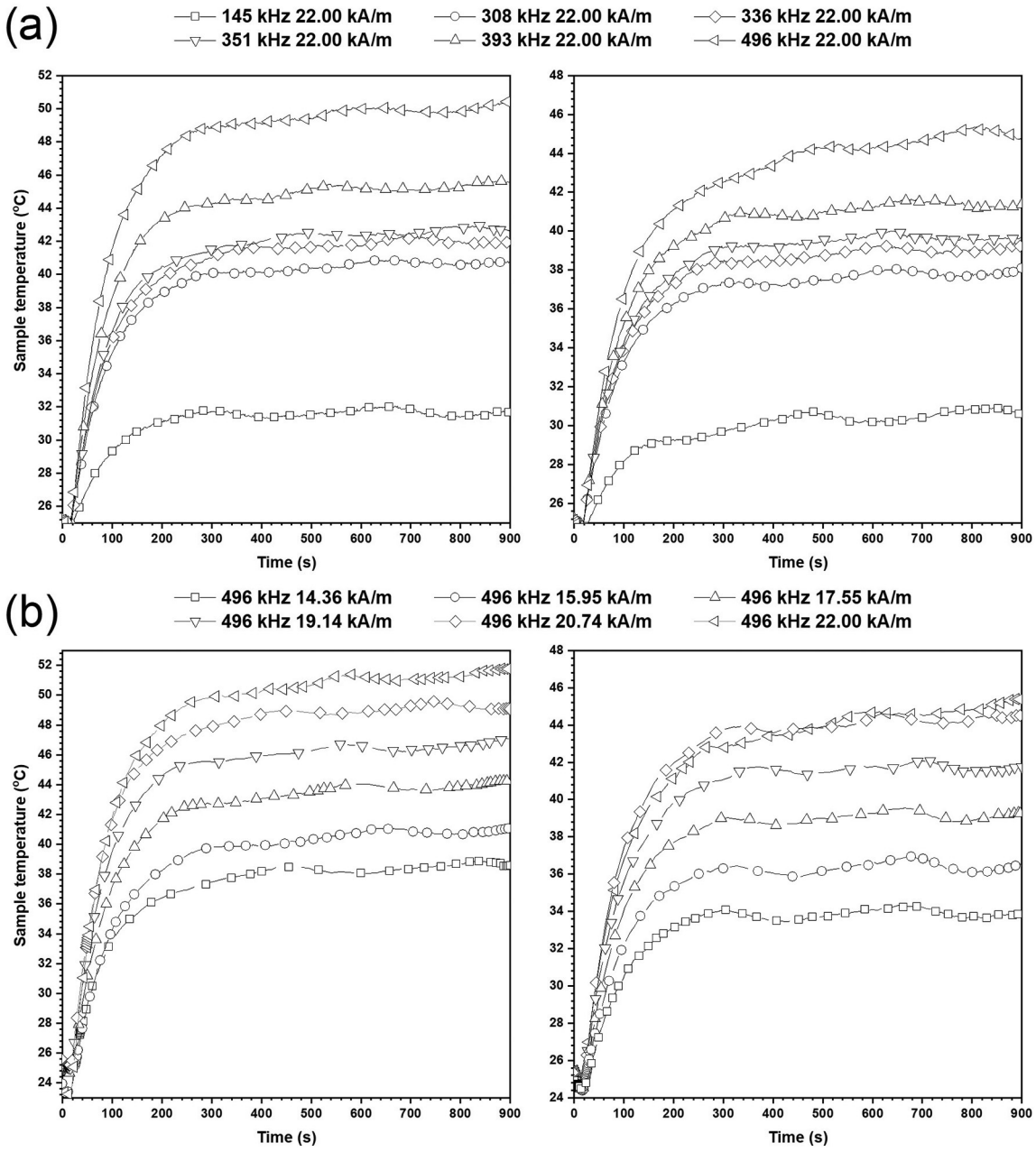

Fig. 8. AMF frequency (a) and field intensity (b) dependencies on the heat generation of the ternary hybrids. On the left side panel results for hybrids with HAp-incorporated MNPs, on the right side – for hybrids with curdlan-incorporated MNPs. Measurements were performed on dry composites. Concentration of MNPs in hybrid was 1 mg/g of dry composite weight.

incorporation type (Table 1).

It is interesting to note that upon laser and dual mode stimulation of dry samples comparable *SAR* values were obtained (above 2500 W/g). While variation of *SAR* was found for MNPs incorporated in ceramic and polymer phase. Similarly, quick and effective sample heating was observed on dry $MnFe_2O_4$ nanoparticles with NIR stimulation [17]. We noticed also a significant difference in wet hybrids temperature behavior. The evaluation of hybrids behavior in Ringer's solution is important due to two facts. First, after the implantation the material will absorb the body tissue fluid; therefore, it is important to predict the heat generation of MNPs-loaded biomaterial soaked in the solution resembling that found in human body. Second, many polymer-based implants are prone for swelling during or soon after the implantation into living tissue. This may generate the excessive long-lasting pressure inside the implantation site, thus negatively affecting the processes of bone formation. For that reason, hybrid material incubation in protein-free medium prior to the implantation may minimize the risk of post-operative complications [34–36]. Therefore, it is of high importance to study the effectiveness of the sample heat induction under conditions as close as possible to real procedures prior *in vivo* experiments. Actually, we did not find in the literature any results dealing with estimation of the heating performance on wet MNPs-loaded biomaterials. In addition, binary HAp/curdlan composite becomes flexible and highly surgically handible after immersion in some liquid anyway [39]. It assures the protection against an excessive sample swelling prior to implementation. Presence of aqueous solvent (due to soaking) with high specific heat inside of porous microstructure acts as an effective coolant changing the composite temperature characteristic. We did observe a mass increase of the hybrids after Ringer's solution treatment. The estimated mass of wet scaffolds was presented in Table 2. One can see that the

Table 1
Calculated values of *dT/dt* and *SAR* for the composite materials depending on the MNPs phase incorporation and stimulation type.

Dry ternary hybrids			Ringer immersed hybrids	
Stimulation	*dT/dt* (°C/s)	*SAR* (W/g)	*dT/dt* (°C/s)	*SAR* (W/g)
HAp-incorporated MNPs				
AMF	0.39	421[a]	0.06	382[c]
LASER	2.40	2592[a]	0.42	2682[c]
DUAL	2.56	2765[a]	0.64	4088[c]
Curdlan-incorporated MNPs				
AMF	0.31	347[b]	0.05	313[d]
LASER	2.71	3035[b]	0.38	2382[d]
DUAL	2.71	3035[b]	0.51	3197[d]

[a] $C_{(I)}$ – 1.08 J/g°C.
[b] $C_{(II)}$ – 1.12 J/g°C.
[c] C_{av} – 2.82 J/g°C.
[d] C_{av} – 2.81 J/g°C.

amount of solvent in respect to the dry material is significant and lowers effective concentration of MNPs (in w/w ratio sense). Therefore, in this case synergic action of both stimuli will be more meaningful. We would like to emphasize that both MNPs incorporation types result in highly efficient energy converting materials. The average ΔT for dry samples under AMF is 30 °C, with NIR 45 °C, and dual mode 77 °C. Compared to wet composites ΔT was found to be 10 °C (AMF), 13 °C (laser) and 24 °C (synergy). Please note that the starting measuring temperature was always close to 24 °C. General conclusion can be drawn that it is possible to achieve temperature treatment regime on wet hybrids even at low content of MNPs and its increase will result in enhancement of maximum composite temperature. The efficacy of heat generation by ternary hybrids in relation to both MNPs concentration and MNPs introduction mode was studied for dry and Ringer's soaked samples (Fig. 9).

We did not monitor any temperature change of the control binary hybrid under action of AMF which gives a direct evidence that heating occurs only due to the presence of magnetic material. Temperature increase of the reference scaffold upon laser exposure was caused by manganese cations NIR absorption as indicated by diffuse reflectance spectra and composite color (Figs. 5, 6a and S4). Addition of the MNPs into hybrids significantly improves heating effect. MNPs contribution becomes extremely important in the case of the Ringer's soaked materials assuring desired temperature response. What might be of possible interest is that we did also a test of cooling behavior of dry and wet ternary composites right after removal of stimuli (see supplementary file S7 and S8). One can note that samples start to reduce their temperature quite rapidly (in comparable manner with gaining temperature), consequently heat dissipation is effective as well. This composite feature is advantageous since temperature response on stimuli is fast emphasizing their effectiveness either in terms of energy conversion and heat dissipation. The effect is strictly limited to the action time of the AMF and NIR. In fact, optimization of the final temperature can be performed in a multidimensional manner through control of AMF (frequency, field intensity), laser optical density (laser power and distance), MNPs concentration and nanoparticle incorporation phase. This can allow for coverage of broad temperature range necessary for final treatment or stimulation of regenerative processes. For instance, hyperthermia treatment (41–48 °C) leads to the protein denaturation, cell function inactivation, oxidative stress or rapid necrotic cell death but above 48 °C highly efficient and risky cancer cell ablation can occur. Whereas, below 41 °C stimulation of the different regenerative process can be effective through enhancement of cell functions (improved blood flow, delivery of drugs and metabolites) [66,67]. It is also worth noting that in almost all cases the maximum time necessary to achieve system temperature saturation does not exceed 300 s. This is crucial, since it is possible to limit exposure time of biological objects for action of the AMF and NIR radiation reducing side effects. The thermovision images showing energy conversion of chosen stimuli into heat on ternary and control binary hybrids are presented in Figs. 10 and 11.

3.1.6. Mechanical properties of the binary and ternary hybrids

The main reason for the mechanical tests was to evaluate the potential changes in compressive behavior of the composites due to the modification with MNPs because such an effect of NPs on the mechanical behavior has been suggested in many works [68,69] Representative curves serving as the basis of the calculations are presented in Fig. 12. It was found that compressive strength of ternary composites did not significantly change when nanoparticles were incorporated in HAp phase for both strain rates. Some of obtained data suggest that modification of the composite with nanoparticles by their incorporation into ceramic phase even decreases mechanical properties of biomaterial. However, when nanoparticles were incorporated into polymer phase, the compressive strength increased in comparison with control (statistically different for P2 for both strain rates and for P1 for 10 mm/min) (Fig. 13a). The Young's modulus has significantly changed only for composites version loaded with higher dose of nanoparticles. For composite with polymer-loaded MNPs this parameter increased for both strain rates while for the composite with HAp-loaded MNPs it decreased for 10 mm/min strain rate (Fig. 13b). Such an effect of NPs on the mechanical behavior of has been confirmed in many works [68,69]. Islam [70] has found that in relation to silica-epoxy nanocomposites (with rigid nanoparticles), the Young's modulus and compressive strength increased with increasing the particle loading. Ondreas [71] suggested that the strengthening effect of nanoparticles on polymeric network is the most striking when nanoparticles dispersion is high. For that point of view it seems that incorporation of MNPs into polymeric phase of the ternary hybrid composite results in strengthening of the whole network of the material and therefore it is beneficial for mechanical properties of ternary composite.

The non-relaxed relative stress (σ_w) is the value which represents viscoelastic behavior of materials. Values close to one indicate the elastic nature of the material, while close to zero indicate viscous flow. For ternary composites tested in presented experiments it was observed that the incorporation of MNPs into polymeric phase has significantly reduced the σ_w value. This indicated the increase of the polymeric matrix viscosity and simultaneously reduction of the susceptibility to

Table 2
Mass change of the ternary hybrids before and after soaking with Ringer's solution (whole composites mass).

Sample	MNPs content in hybrids (mg/g):					
	0.75	1	1.25	1.50	1.75	2
MNPs in HAp mass of composite (g)	0.7587	0.7383	0.8659	0.9122	0.8403	0.7518
MNPs in HAp mass after soaking (g)	1.7155	1.6746	1.9819	1.9607	1.9714	1.7177
Ringer solution content (g)	0.9568	0.9363	1.116	1.0485	1.1311	0.9659
MNPs in polymer mass of composite (g)	0.8007	0.7231	0.8263	0.8011	0.9244	0.8278
MNPs in polymer mass after soaking (g)	1.8376	1.6127	1.8505	1.7949	1.9986	1.7667
Ringer solution content (g)	1.0369	0.8896	1.0242	0.9938	1.0742	0.9389

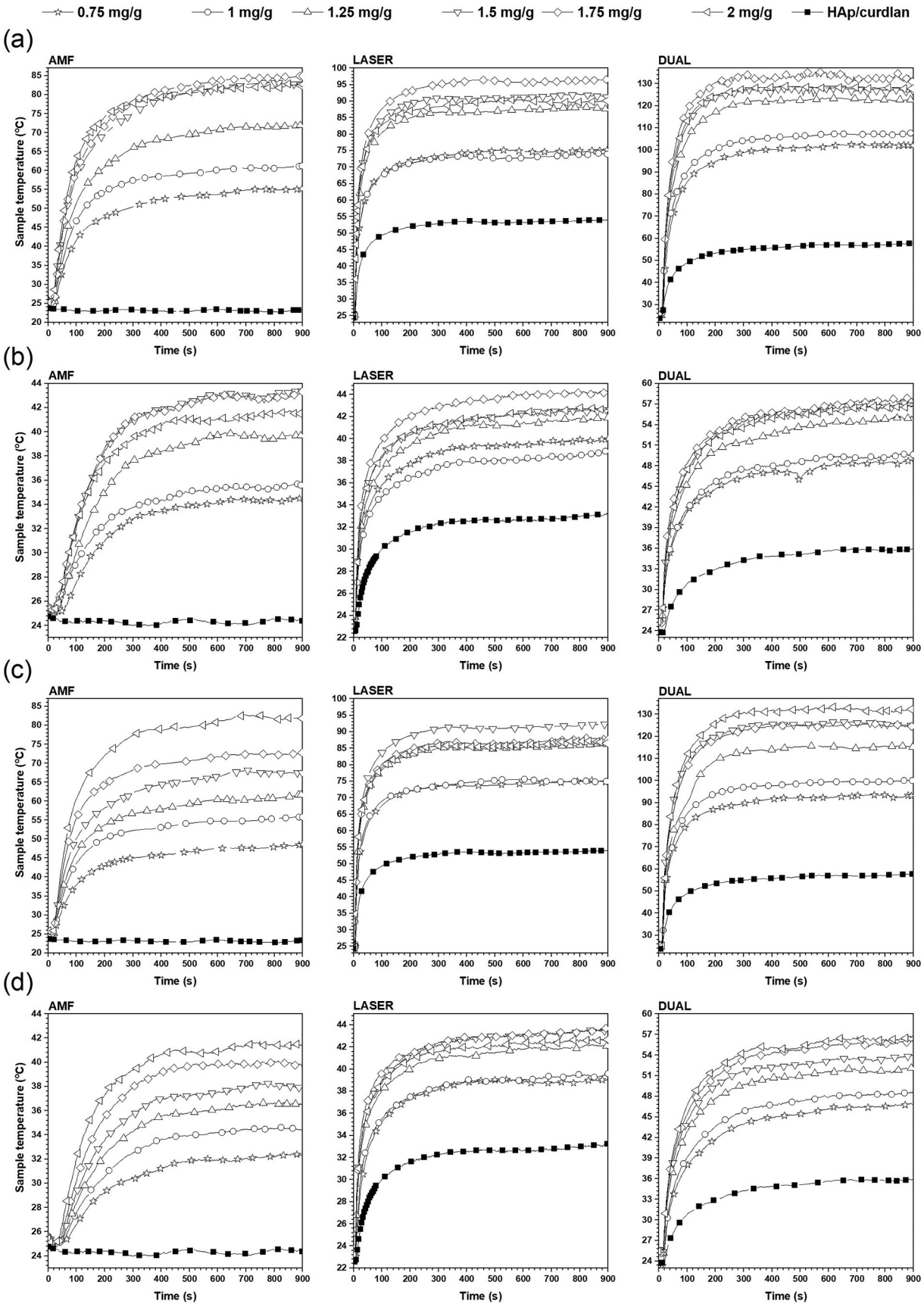

Fig. 9. Heat induction of the ternary hybrids under action of AMF (left), NIR laser (middle) and DUAL mode (right) for sets of (a) dry hybrids with HAp-incorporated MNPs; (b) hybrids with HAp-incorporated MNPs immersed in Ringer solution; (c) dry hybrids with curdlan-incorporated MNPs, (d) hybrids with curdlan-incorporated MNPs immersed in Ringer solution. All measurements were done as a function of the MNPs content (in mg/g of dry composite weight).

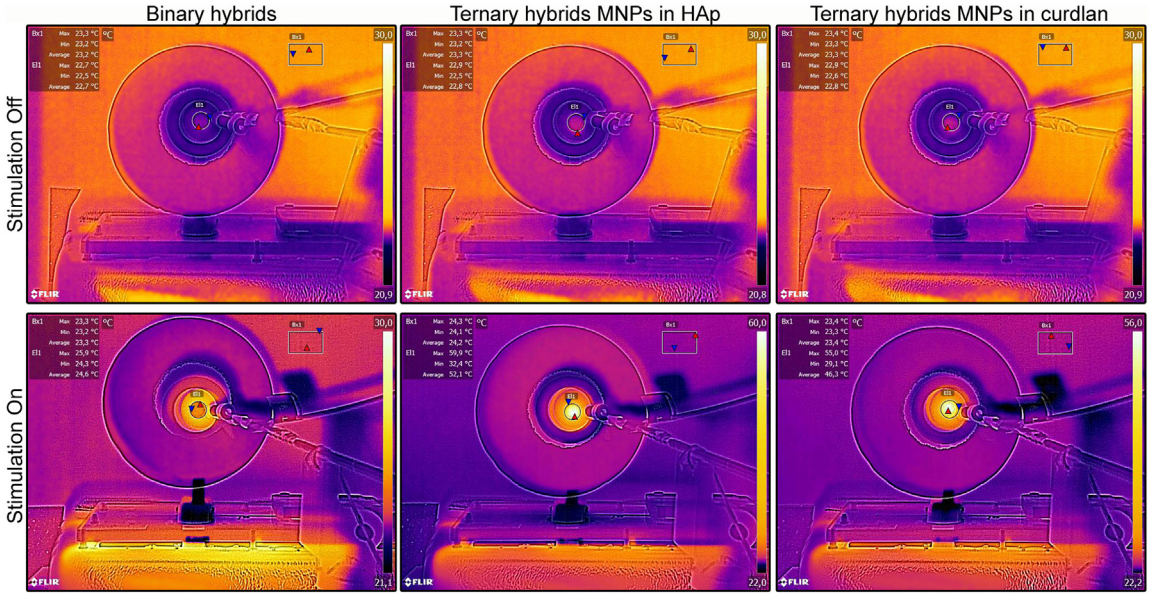

Fig. 10. Thermovision images of the effect of heat induction on reference sample (left) as well as hybrids with HAp-incorporated MNPs (middle), curdlan-incorporated MNPs (right) under AMF action.

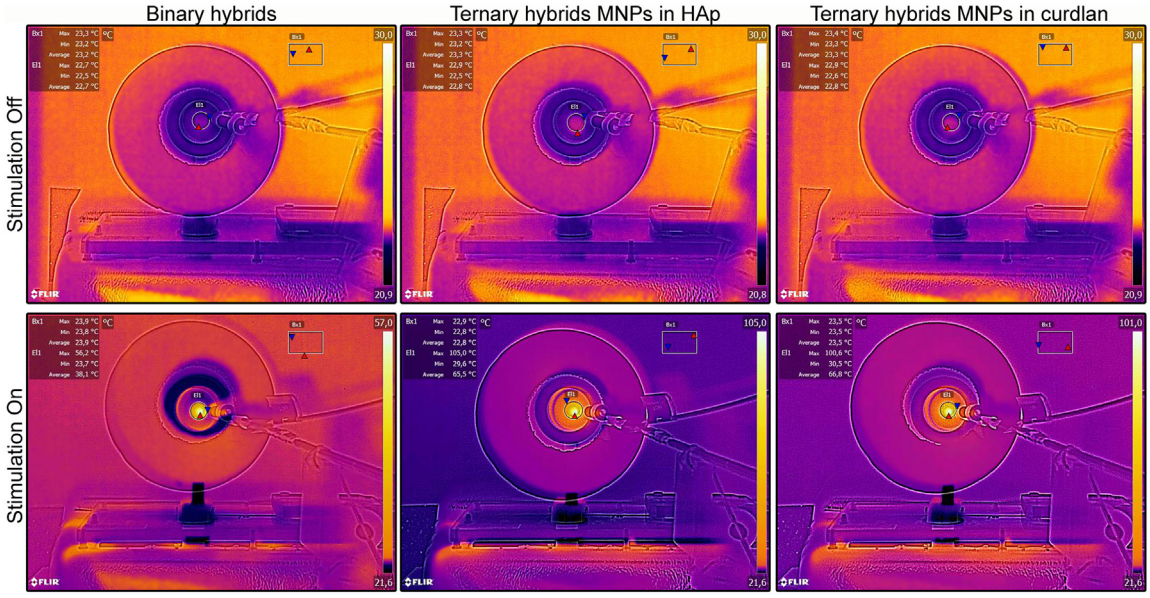

Fig. 11. Thermovision images of the effect of heat induction on reference sample (left) as well as hybrids with HAp-incorporated MNPs (middle), curdlan-incorporated MNPs (right) under dual stimulation mode.

plastic deformation. It was also observed that higher strain rates generate lower values of non-relaxed relative stress (Fig. 13c). This indicated a lower material viscosity due to a higher deformation rate. Furthermore, the material retains a high "potential" for relaxation. In turn, at low deformation rates, relaxation occurs already during compression, and the material exhibits more elastic behavior.

All these results strongly suggest the impact of MNPs on mechanical behavior of HAp/curdlan composites when nanoparticles are incorporated into polymeric phase. Such method of modification was also beneficial for thermal properties of ternary composite. It should be noted that incorporation MNPs into HAp phase in general did not significantly alter these properties; therefore such a method of the composite modification with MNPs is less recommended for synthesis of materials useful in temperature-dependent therapy.

3.1.7. MNPs release from the ternary composite

The results presented in this report clearly show that flexible HAp/curdlan composite for bone tissue regeneration, enriched with magnetite nanoparticles, could be a powerful tool in medicine. Ternary composites after the implantation into bone defects may be stimulated by different conditions (AMF, NIR and the combination of the above mentioned) to increase the local implant temperature in a controlled manner. At least two potential applications may be proposed for such biomaterials. First, ternary composite can be used for enhanced regeneration of bone tissue in bone defects because the implant's temperature can be raised to the values below 41 °C (diathermia regime). This in turn can stimulate the regenerative and therapeutic processes (causing the vasodilation and enhancement of the nutrients and oxygen transport into the regeneration site). It was already shown that the HAp scaffolds enriched with commercial Fe_3O_4 particles can effectively stimulate the formation of the new bone through osteogenesis promotion.

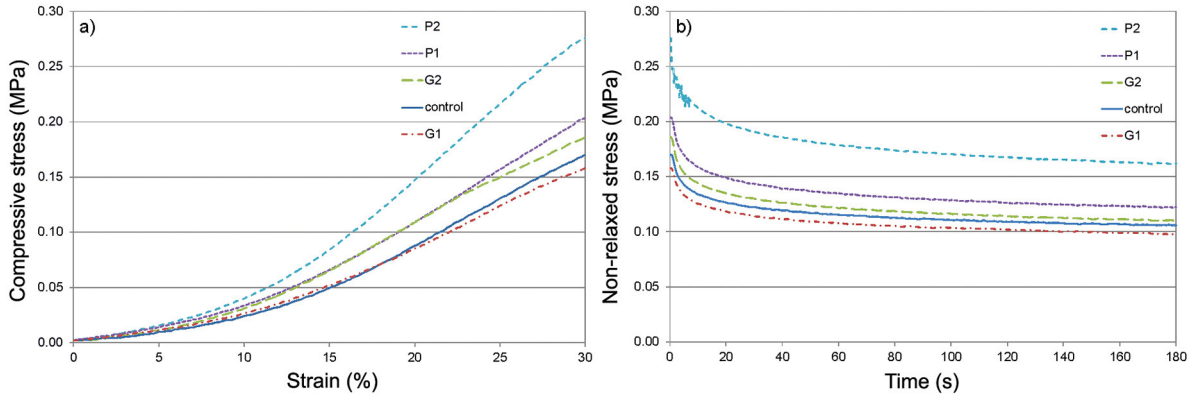

Fig. 12. Mechanical behavior of tested composites - representative curves for strain rate of 0,5 mm/min. Symbols of the samples: C – control binary composite; G1 and G2 – ternary composite with HAp-incorporated MNPs, with 1 or 2 mg of MNPs per gram of dry composite weight, respectively; P1 and P2 – ternary composite with polymer-incorporated MNPs, with 1 or 2 mg of MNPs per gram of dry composite weight, respectively.

This strategy could be beneficial for bone tissue regeneration in patients suffering from illnesses which impair the bone tissue healing, such as osteoporosis or diabetes mellitus, due to the accompanying vascular and immune deficiencies. Second, the ternary composite can be used for the treatment of recurring bone cancer in bone defect created after the removal of primary bone cancer. During the postoperative period the implanted composite can serve first as a scaffold for bone tissue regeneration. However, if the recurrence of the cancer occurs, local temperature of the implant could be immediately raised above 43 °C to induce the controlled apoptosis of cancer cells. Similar strategy was proposed by Andronescu et al. for the application of collagen-HAp-magnetite composite [19].

Magnetite-enriched ternary composite could be effective for such applications only if the magnetite nanoparticles are loaded to the biomaterial in relatively stable way. Therefore, we checked the stability of nanoparticle loading during incubation of ternary composites (with MNPs incorporated both into ceramic or polymeric phases and with various MNPs content) in buffers of pH 7.4 and 6.5, for 6 weeks. pH 6.5 was selected on a basis of literature data concerning the extracellular pH of solid tumors [72] while pH 7.4 corresponds to pH in healthy bone

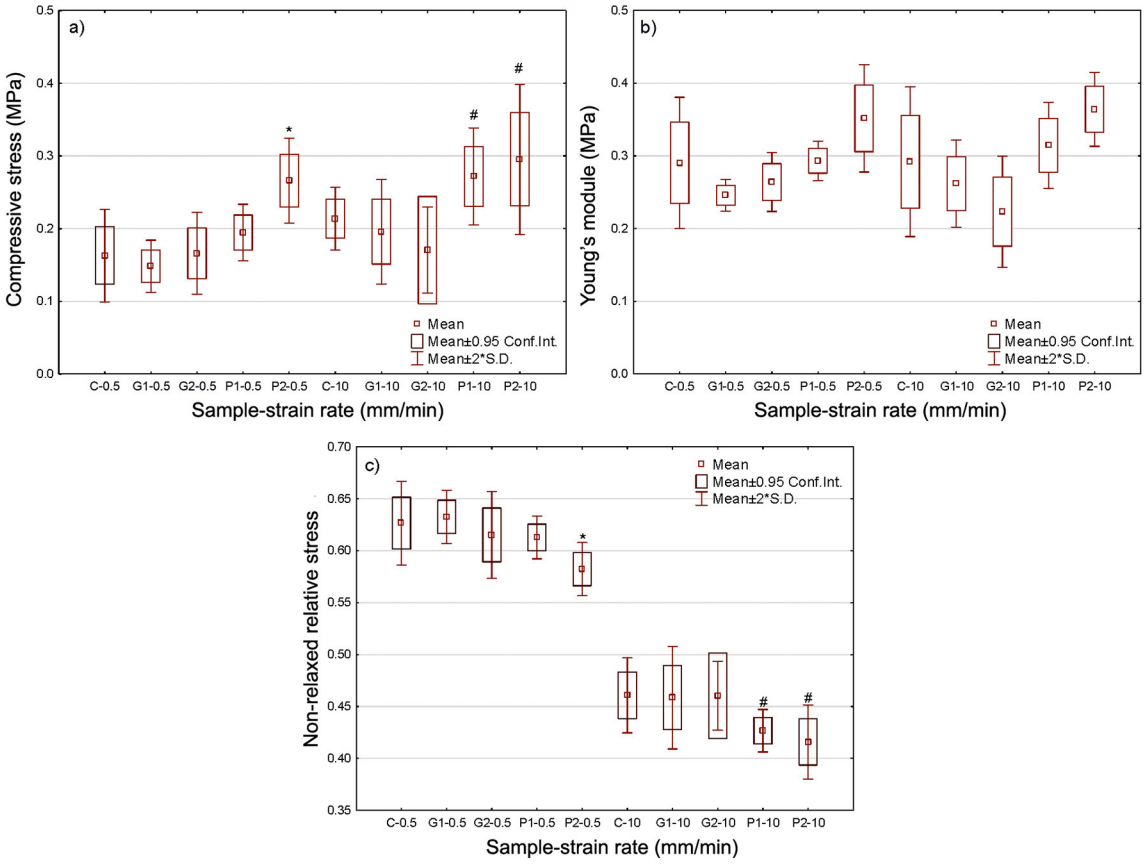

Fig. 13. Mechanical properties of tested composites at 2 different strain rates: a) compressive strength, b) Young's modulus, c) the rate of non-relaxed relative stress (σ_w). Symbols of the samples: C – control binary composite; G1 and G2 – ternary composite with HAp-incorporated MNPs, with 1 or 2 mg of MNPs per gram of dry composite weight, respectively; P1 and P2 – ternary composite with polymer-incorporated MNPs, with 1 or 2 mg of MNPs per gram of dry composite weight, respectively. Symbols (*) and (#) denote statistically significant differences in relation to C-0.5 and C-10, respectively.

Table 3
Amount (%) of MNPs released (as mean and SD) from ternary hybrids after 6 weeks of incubation in buffers pH 6.5 and pH 7.4.

Composites/pH of buffer	MNPs content in hybrids (mg/g):					
	0.75	1	1.25	1.50	1.75	2
With HAp-incorporated MNPs/pH 6.5	10.6 ± 0.27	8.5 ± 0.19	10.2 ± 0.16	4.9 ± 0.00	6.3 ± 0.11	3.7 ± 0.08
With polymer-incorporated MNPs/pH 6.5	9.2 ± 0.27	5.8 ± 0.26	7.1 ± 0.16	5.4 ± 0.00	5.0 ± 0.11	2.5 ± 0.01
With HAp-incorporated MNPs/pH 7.4	9.5 ± 0.00	5.2 ± 0.09	5.5 ± 0.11	4.4 ± 0.210	2.7 ± 0.04	2.3 ± 0.11
With polymer-incorporated MNPs/pH 7.4	8.9 ± 0.00	6.0 ± 0.09	5.8 ± 0.06	3.5 ± 0.00	2.3 ± 0.00	3.1 ± 0.06

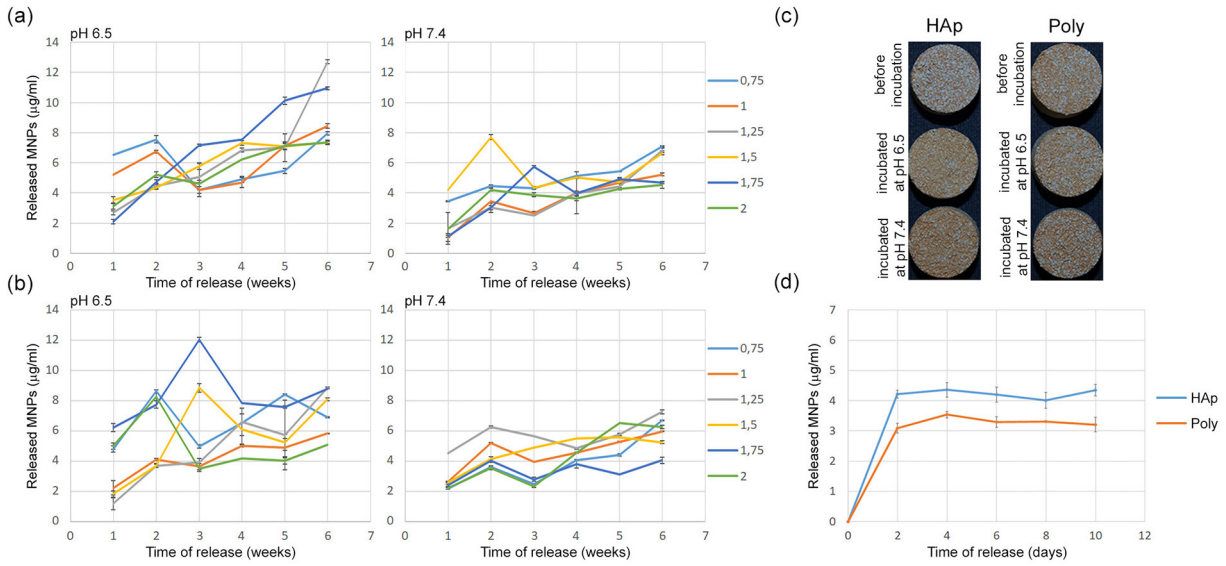

Fig. 14. Profiles of the MNPs release to Sorenson's buffer of different pH from hybrids with HAp-incorporated MNPs (a), hybrids with curdlan-incorporated MNPs (b), images of the scaffolds before and after incubation (c) as well as profile of MNPs release to human serum (d).

tissue. Samples of the buffers were aseptically collected every week and evaluated spectrophotometrically at 370 nm. This wavelength was chosen on the basis of our pilot experiments (data not shown) and is close to the value selected from our previous reports. The results were presented in Table 3 and Fig. 14. The release profiles show that MNPs are released slowly and at relatively low level, varying between 1 and 7 µg/ml during the first week and 4–13 µg/ml during the sixth week of experiment (Fig. 14). It is therefore concluded that during the prolonged incubation period, the release of MNPs would remain at comparable low level. There is no notable correlation between the amounts of loaded and released MNPs. The fluctuations in the concentrations of released MNPs within the entire incubation period may result from the re-precipitation of the particles on the composite surfaces. Table 3 shows the final amounts of the released MNPs (after 6 weeks of incubation) as a percent of their amounts initially loaded into the composites. Some interesting observations may be drawn on basis of these data.

First, the amount of the particles released from all composite samples did not exceed 10.6% of their starting quantity. Therefore, majority of MNPs remained within the hybrids during the experiment. Second, for both composites with HAp- or curdlan-incorporated MNPs, more nanoparticles were released at pH 6.5 than at pH 7.4. Thus, more stable composite incorporation is expected during the implantation into healthy bone tissue (conditions predicted for the surgical procedure and post-operative treatment) than in the case of cancer recurrence. Third, according to general observation, the larger is the initial amount of incorporated MNPs, the smaller is the percent of released particles. It seems possible that MNPs aggregate during the synthesis of hybrids with the intensity related to their initial concentration. If this hypothesis is true, the aggregated MNPs within the composites would consequently generate less mobile nanoparticles. Fourth, it seems that the MNPs incorporation mode slightly influences the release of particles to the medium, being higher in the case of HAp-incorporated version (Table 3). This might be caused by the weak binding forces between MNPs and HAp granules since they have not been sintered together. This could explain the more intense elution of MNPs from hybrids with HAp-incorporated particles that from those with curdlan-incorporated particles. This would also support our earlier hypothesis that curdlan polymer may serve as the layer protecting the MNPs from the release and also suppressing the heat generating ability of the fabricated materials. This hypothesis can be also supported by observations based on the images of ternary composites after 6 weeks of incubation in buffers (pH 6.5 and 7.4) (Fig. 14).

While hybrids with curdlan-incorporated MNPs look the same before and after incubation, these with HAp-incorporated MNPs are slightly different before and after the incubation (Fig. 14). It seems that MNPs in the latter type of hybrid underwent a redistribution within the matrix, probably due to the release and subsequent re-precipitation of MNPs within the scaffold. This enhances the probability of our earlier speculations concerning the precipitation of released MNPs particles. The amount of released/lost MNPs is that small that it did not affect the temperature behavior of scaffolds significantly (Fig. S11). We also checked whether the action of different stimuli could potentially cause the MNPs release (see Fig. S10). The supernatants were taken after the heat generation and absorption spectra were measured showing the flat line. Thus it was concluded that during the hybrid exposure to both AMF and NIR under dual mode (the strongest temperature effect) there is no risk of MNPs release. In physiological conditions, however, tissue liquids contain a certain quantity of proteins which alter the viscosity of body fluids in comparison with buffered saline. Such media may impair the movement of NPs from solid matrices and therefore prevent the rise of the desired temperature in induced composite. To verify this effect in

conditions the most imitating the natural body environment, samples of ternary composites were incubated in Ringer's solution of pH 7.4 supplemented with 10% human serum. Some release of magnetic nanoparticles was observed on second day of the experiment; then the level of MNPs in the liquid remained at similar lever for the period of 10 days (Fig. 14d). Also the brownish color of incubated composites did not change during this period (data not shown) indicating that majority of composite-entrapped MNPs remained within the material's network. The overall level of MNPs release from these samples was 4.36% and 3.54% of total MNPs amount for the composite with HAp- and curdlan-incorporated MNPs, respectively (Fig. 14d). Therefore, the presence of human serum proteins in environment did not significantly alter the stability of MNPs entrapped within the composites.

4. Conclusions

The ternary hydroxyapatite/curdlan/nanomagnetite hybrids with different incorporation of the MNPs *i.e.* into ceramic and polymer phase were fabricated. Their energy conversion ability by using AMF, NIR and synergic action of both stimuli on dry and wet scaffolds was evaluated. We have shown that it is possible to achieve efficient heating of hybrids under relatively short exposure time (below 2 min) assuring temperature regime adequate for the stimulation of the regenerative processes as well as hyperthermia keeping the low MNPs content (1 mg/g MNPs *vs*. HAp and curdlan). The overall effect can be modulated *via* change of AMF/NIR parameters and can be greatly enhanced by concentration of the MNPs. This can allow for control over the broad temperature range depending on the treatment aim as well as can be used for protection against overheating. We would like to emphasize that the part of the results have been obtained on wet hybrids (Ringer's solution soaking) in order to mimic *in situ* conditions and their heating ability was still high enough especially in the case of synergic effect of AMF and NIR. The concentration of the MNPs in the scaffolds was relatively low upon comparison with other reports [10,11,24,31], thus any possible adverse effects connected with particle release can be minimized. Analysis of the MNPs release into buffers showed that after prolonged time (6 weeks) the concentration of the free particles is below 15 μg/ml. Therefore, the majority of incorporated MNPs remained within the hybrids during the experiments. Similar conclusion can be drawn after hybrids exposed to presence of human serum proteins in environment – it did not significantly altered the stability of MNPs entrapped within the composites. This observation is promising for possible application of ternary composites because, in contrast to abundant literature data, the cytotoxic effects of magnetite (Fenton's reaction or other) will be off concern. The heat generation after release studies was slightly lower but had no significant effect on the scaffolds temperature behavior showing their good stability over time in the biological media. More interestingly we found that the mechanical properties of the hybrids with MNPs incorporation into the curdlan (polymer phase) are improved due to the increase of compressive strength and Young's modulus leading to overall strengthening of the whole network. While addition of MNPs into HAp granules (ceramic phase) did not cause meaningful changes in respect to control binary hybrid.

CRediT authorship contribution statement

Hereby, I declare that following authors contributed to the article entitled as *Efficient non-contact heat generation on flexible, ternary hydroxyapatite/curdlan/nanomagnetite hybrids for temperature controlled processes*, Magdalena Kulpa-Greszta, Robert Pązik, Patrycja Kłoda, Anna Tomaszewska, Emilia Zachanowicz, Krzysztof Pałka, Grazyna Ginalska, Anna Belcarz submitted to Materials Science and Engineering C in the following manner:

M.K.-G. – conducted of experiments with AMF and NIR laser stimulation, data analysis, discussion and manuscript writing;

R.P. – main idea, writing manuscript, final corrections and editing, data analysis;

P. K. – synthesis of MNPs, material characterization FT-IR-ATR, XRD, data analysis, discussion and manuscript writing;

A. T. – material characterization DRS, DLS, optical microscopy of hybrids, data analysis, discussion and manuscript writing;

E.Z. – DSC measurements and data analysis, discussion of results;

K.P. – measurement and evaluation of hybrid mechanical properties, discussion of results;

G.G. – analysis of hybrids properties, discussion and manuscript writing;

A.B. – main idea, synthesis of HAp, preparation of all hybrid materials, MNPs release measurements, data analysis, discussion and manuscript writing.

Declaration of competing interest

The authors declare that they have no known competing financial interests or personal relationships that could have appeared to influence the work reported in this paper.

Acknowledgements

Financial support of the National Science Centre in course of realization of the Project no. UMO-2017/25/B/ST5/00497 is gratefully acknowledged. We also express our gratitude to Medical Inventi Joint stock Company for the allowance to use their patented procedure of binary composite synthesis and for providing the compounds for its production. Financial assistance was partially provided by Ministry of Science and Higher Education in Poland within DS2 project of Medical University of Lublin. The authors would like to thank Prof. Grzegorz Litwinienko (University of Warsaw) for TGA measurement of the MNPs sample as well as Andrzej Dziedzic (University of Rzeszów) for TEM characterization.

Appendix A. Supplementary data

Supplementary data to this article can be found online at https://doi.org/10.1016/j.msec.2020.111360.

References

[1] P. Ducheyne, Q. Qiu, Biomaterials. 20 (1999) 2287–2303.
[2] M.H. Fathi, A. Hanifi, V. Mortazavi, J. Mater. Process. Technol. 202 (2008) 536–542.
[3] H. Oonishi Jr., H. Oonishi, H. Ohashi, I. Kawahara, Y. Hanaoka, L.L. Hench, Advanced, in: B. Ben-Nissan (Ed.), Calcium Phosphate Biomaterials, Springer-Verlag Berlin Heidelberg, 2014, pp. 19–49.
[4] R.Z. Legeros, C.A. Garrido, S.E. Lobo, F.M. Turíbio, Int. J. Biomater. 2011 (2011) 129727.
[5] J.K. Ku, I. Hong, B.K. Lee, P.Y. Yun, J.K. Lee, J. Korean Assoc, Oral Maxillofac. Surg. 45 (2019) 51–67.
[6] I. Salma, G. Salms, M. Pilmane, D. Loca, J. Locs, N. Romanchikova, A. Skagers, L. Berzina Cimdina, J. Oral Maxillofac. Surg. 40 (2011) 1216.
[7] E. Peng, F. Wang, J.M. Xue, J. Mater. Chem. B 3 (2015) 2241–2276.
[8] L. Lartigue, P. Hugounenq, D. Alloyeau, S.P. Clarke, M. Le, R. Bazzi, D.F. Brougham, C. Wilhelm, F. Gazeau, ACS Nano 12 (2012) 10935–10949.
[9] A. Espinosa, R. Di Corato, J. Kolosnjaj-Tabi, P. Flaud, T. Pellegrino, C. Wilhelm, ACS Nano 10 (2016) 2436–2446.
[10] J.J. Kim, R.K. Singh, S.J. Seo, T.H. Kim, J.H. Kim, E.J. Lee, H.W. Kim, RSC Adv. 4 (2014) 17325–17336.
[11] M. Banobre-Lopez, Y. Pineiro-Redondo, M. Sandri, A. Tampieri, R. De Santis, V.A. Dediu, J. Rivas, IEEE Trans. Magn. 50 (2014) 5400507.
[12] T. Ota, Y. Nishida, K. Ikuta, R. Kato, E. Kozawa, S. Hamada, T. Sakai, N. Ishiguro, PLoS One 12 (2017) 1–16.
[13] D. Jaque, L. Martínez Maestro, B. del Rosal, P. Haro-Gonzalez, A. Benayas, J.L. Plaza, E. Martín Rodríguez, J. García Solé, Nanoscale. 6 (2014) 9494–9530.
[14] Y. Zhang, Y. Zhai, in: S. Grundas (Ed.), Advances in Induction and Microwave Heating of Mineral and Organic Material, InTech, 2011: pp. 483–500.
[15] H.I. Bicher, F.W. Hetzel, T.S. Sandhu, S. Frinak, P. Vaupel, M.D. O'Hara, T. O'Brien, Radiology. 137 (1980) 523–530.
[16] D. Jaque, F. Vetrone, Nanoscale. 4 (2012) 4301–4326.
[17] R. Pązik, E. Zachanowicz, B. Poźniak, M. Małecka, A. Zięcina, Ł. Marciniak, RSC Adv. 7 (2017) 18162–18171.

[18] T. Miyazaki, M. Kawashit, C. Ohtsuki, Handbook of Bioceramics and Biocomposites, Springer International Publishing, Switzerland, 2016, pp. 287–300.
[19] E. Andronescu, M. Ficai, G. Voicu, D. Ficai, M. Maganu, A. Ficai, J. Mater. Sci. Mater. Med. 21 (2010) 2237–2242.
[20] S. Torgbo, P. Sukyai, Mater. Chem. Phys. 237 (2019) 121868.
[21] M. Yadav, K.Y. Rhee, S.J. Park, D. Hui, Compos. Part B Eng. 66 (2014) 89–96.
[22] A. Tampieri, M. Iafisco, M. Sandri, S. Panseri, C. Cunha, S. Sprio, E. Savini, M. Uhlarz, T. Herrmannsdörfer, ACS Appl. Mater. Interfaces 6 (2014) 15697–15707.
[23] F. Heidari, M. Razavi, M.E. Bahrololoom, M. Yazdimamaghani, M. Tahriri, H. Kotturi, L. Tayebi, Ceram. Int. 44 (2018) 275–281.
[24] T. Iwasaki, R. Nakatsuka, K. Murase, H. Takata, H. Nakamura, S. Watano, Int. J. Mol. Sci. 14 (2013) 9365–9378.
[25] H.H. Beherei, M.S. Abdel-Aal, A.A. Shaltout, A. El-Magharby, Der. Pharma. Chem. 4 (2012) 544–551.
[26] V.T. Le, V.D. Doan, D.D. Nguyen, H.T. Nguyen, Q.P. Ngo, T.K.N. Tran, H.S. Le, Water Air Soil Pollut. 229 (2018) 101.
[27] P. Hou, C. Shi, L. Wu, X. Hou, Microchem. J. 128 (2016) 218–225.
[28] H.M. Yun, S.J. Ahn, K.R. Park, M.J. Kim, J.J. Kim, G.Z. Jin, H.W. Kim, E.C. Kim, Biomaterials. 85 (2016) 88–98.
[29] A. Gloria, T. Russo, U. D'amora, S. Zeppetelli, T. D'Alessandro, M. Sandri, M. Bañobre-López, Y. Piñeiro-Redondo, M. Uhlarz, A. Tampieri, J. Rivas, T. Herrmannsdörfer, V.A. Dediu, L. Ambrosio, R. De Santis, J. R. Soc. Interface 10 (2013) 20120833.
[30] H. Kakwere, M.P. Leal, M.E. Materia, A. Curcio, P. Guardia, D. Niculaes, R. Marotta, A. Falqui, T. Pellegrino, ACS Appl. Mater. Interfaces 7 (2015) 10132–10145.
[31] S. Sprio, S. Panseri, A. Adamiano, M. Sandri, M. Uhlarz, T. Herrmannsdorfer, E. Landi, Y. Pineiro-Remondo, A. Tampieri, Front. Nanosci. Nanotechnol. 3 (2017) 1–9.
[32] M. Ngiam, S. Liao, A.J. Patil, Z. Cheng, C.K. Chan, S. Ramakrishna, Bone. 45 (2009) 4–16.
[33] F. Heidari, M. Razavi, M.E. Bahrololoom, R. Bazargan-Lari, D. Vashaee, H. Kotturi, L. Tayebi, Mater. Sci. Eng. C 65 (2016) 338–344.
[34] L. Borkowski, M. Pawłowska, R.P. Radzki, M. Bieńko, I. Polkowska, A. Belcarz, M. Karpiński, T. Słowik, L. Matuszewski, A. Slósarczyk, G. Ginalska, Mater. Sci. Eng. C 53 (2015) 60–67.
[35] L. Borkowski, M. Kiernicka, A. Belcarz, K. Pałka, M. Hajnos, G. Ginalska, J. Biomed. Mater. Res. - Part B Appl. Biomater. 105 (2017) 1178–1190.
[36] L. Borkowski, T. Lübek, M. Jojczuk, A. Nogalski, A. Belcarz, K. Palka, M. Hajnos, G. Ginalska, J. Biomed. Mater. Res. - Part B Appl. Biomater. 106 (2018) 2653–2664.
[37] P.Z. Belcarz A, G. Ginalska, A. Slosarczyk, Bioactive Composite and Process for the Production of the Bioactive Composite, EP 2421570 B1, (2015).
[38] A. Belcarz, G. Ginalska, T. Pycka, A. Zima, A. Slosarczyk, I. Polkowska, Z. Paszkiewicz, W. Piekarczyk, Cent. Eur. J. Biol. 8 (2013) 534–548.
[39] A. Belcarz, A. Zima, G. Ginalska, Int. J. Pharm. 454 (2013) 285–295.
[40] R. Pazik, R. Tekoriute, S. Håkansson, R. Wiglusz, W. Strek, G.A. Seisenbaeva, Y.K. Gun'ko, V.G. Kessler, Chem. - A Eur. J. 15 (2009) 6820–6826.
[41] A. Lewinska, J. Adamczyk-Grochala, D. Bloniarz, J. Olszowka, M. Kulpa-Greszta, G. Litwinienko, A. Tomaszewska, M. Wnuk, R. Pazik, Redox Biol. 28 (2019) 101337.
[42] Z. Paszkiewicz, A. Ślósarczyk, A. Zima, The Method for Production of Highly Porous, Highly Active, Calcium-Phosphate Material for Implantations, PL.210026 (2011).
[43] H.P. Klug, L.E. Alexander, X-Ray Diffraction Procedures: For Polycrystalline and Amorphous Materials, 2nd edition, Wiley, New York, 1974.
[44] C.G. Ramankutty, S. Sugunan, Appl. Catal. A 218 (2001) 39–51.
[45] S.N. Slabzhennikov, O.B. Ryabchenko, L.A. Kuarton, Russ. J. Coord. Chem. 34 (2008) 551–553.
[46] V.G. Kessler, G.I. Spijksma, G.A. Seisenbaeva, S. Håkansson, D.H.A. Blank, H.J.M. Bouwmeester, J. Sol-Gel Sci. Technol. 40 (2006) 163–179.
[47] A.G. Roca, L. Gutiérrez, H. Gavilán, M.E. Fortes Brollo, S. Veintemillas-Verdaguer, M.P. Morales, Adv. Drug Deliv. Rev. 138 (2019) 68–104.
[48] W. Xie, Z. Guo, F. Gao, Q. Gao, D. Wang, B.S. Liaw, Q. Cai, X. Sun, X. Wang, L. Zhao, Theranostics. 8 (2018) 3284–3307.
[49] C. Blanco-Andujar, A. Walter, G. Cotin, C. Bordeianu, D. Mertz, D. Felder-Flesch, S. Begin-Colin, Nanomedicine. 11 (2016) 1889–1910.
[50] R. Pązik, E. Piasecka, M. Małecka, V.G. Kessler, B. Idzikowski, Z. Śniadecki, R.J. Wiglusz, RSC Adv. 3 (2013) 12230.
[51] R. Pązik, A. Lewińska, J. Adamczyk-Grochala, M. Kulpa-Greszta, P. Kłoda, A. Tomaszewska, A. Dziedzic, G. Litwienienko, M. Noga, D. Sikora, M. Wnuk, J. Phys. Chem. B 124 (2020) 4931–4948.
[52] K. Marycz, R. Pazik, K. Zawisza, K. Wiglusz, M. Maredziak, P. Sobierajska, R.J. Wiglusz, Mater. Sci. Eng. C 69 (2016) 17–26.
[53] P. Sobierajska, R. Pazik, K. Zawisza, G. Renaudin, J.-M. Nedelec, R.J. Wiglusz, CrystEngComm. 18 (2016) 3447–3455.
[54] R.J. Wiglusz, Z. Drulis-Kawa, R. Pazik, K. Zawisza, A. Dorotkiewicz-Jach, J. Roszkowiak, J.M. Nedelec, Dalton Trans. 44 (2015) 6918–6925.
[55] R.J. Wiglusz, B. Pozniak, K. Zawisza, R. Pazik, RSC Adv. 5 (2015) 27610–27622.
[56] S.M. Rafigh, A.V. Yazdi, M. Vossoughi, A.A. Safekordi, M. Ardjmand, Int. J. Biol. Macromol. 70 (2014) 463–473.
[57] G.T. Kalyanasundaram, M. Doble, S.N. Gummadi, AMB Express 2 (2012) 1–10.
[58] M. Gaft, R. Reisfeld, G. Panczer, Mineralogy Modern Luminescence Spectroscopy of Minerals and Materials, Springer International Publishing Switzerland, 2015.
[59] C. Paluszkiewicz, A. Slosarczyk, D. Pijocha, M. Sitarz, M. Bućko, A. Zima, A. Chróścicka, M. Lewandowska-Szumieł, J. Mol. Struct. 976 (2010) 301–309.
[60] I. Mayer, O. Jacobsohn, T. Niazov, J. Werckmann, M. Iliescu, M. Richard-Plouet, O. Burghaus, D. Reinen, Eur. J. Inorg. Chem. (2003) 1445–1451.
[61] D.H. Ortgies, F.J. Teran, U. Rocha, L. de la Cueva, G. Salas, D. Cabrera, A.S. Vanetsev, M. Rähn, V. Sammelselg, Y.V. Orlovskii, D. Jaque, Adv. Funct. Mater. 28 (2018) 1–11.
[62] I. Baker, Q. Zeng, W. Li, C.R. Sullivan, J. Appl. Phys. 99 (2006) 97–100.
[63] E. Lima, E. De Biasi, M.V. Mansilla, M.E. Saleta, M. Granada, H.E. Troiani, F.B. Effenberger, L.M. Rossi, H.R. Rechenberg, R.D. Zysler, J. Phys. D. Appl. Phys. 46 (2013) 045002.
[64] L. Gutiérrez, L. De La Cueva, M. Moros, E. Mazarío, S. De Bernardo, J.M. De La Fuente, M.P. Morales, G. Salas, Nanotechnology. 30 (2019) 112001.
[65] M. Vasilakaki, C. Binns, K.N. Trohidou, Nanoscale. 7 (2015) 7753–7762.
[66] H.F. Wang, T.B. Huff, D.A. Zweifel, W. He, P.S. Low, A. Wei, J.X. Cheng, Proc. Natl. Acad. Sci. U. S. A. 102 (2005) 15752–15756.
[67] J.G. Short, P.F. Turner, P Proc. IEEE. 68 (1980) 133–142.
[68] J.M. Corrêa, M. Mori, H.L. Sanches, A.D. Da Cruz, E. Poiate, I.A.V.P. Poiate, Int. J. Biomater. 2015 (2015) 485275.
[69] R. Pokrowiecki, K. Pałka, A. Mielczarek, Nanomedicine. 13 (2018) 639–667.
[70] S. Islam, R. Masoodi, H. Rostami, 2013 (2013) 275037.
[71] F. Ondreas, P. Lepcio, M. Zboncak, K. Zarybnicka, L.E. Govaert, J. Jancar, Macromolecules. 52 (2019) 6250–6259.
[72] A.I. Hashim, X. Zhang, J.W. Wojtkowiak, G.V. Martinez, R.J. Gillies, NMR Biomed. 24 (2011) 582–591.